

Thermodynamic study of binary systems containing sulphur dioxide and nitric oxide: measurements and modelling

Benoit Creton, Carlos Nieto-Draghi, Theodorus de Bruin, Véronique Lachet, Elise Ahmar, Alain Valtz, Christophe Coquelet, Silvia Lasala, Romain Privat, Jean-Noël Jaubert

► **To cite this version:**

Benoit Creton, Carlos Nieto-Draghi, Theodorus de Bruin, Véronique Lachet, Elise Ahmar, et al.. Thermodynamic study of binary systems containing sulphur dioxide and nitric oxide: measurements and modelling. Fluid Phase Equilibria, Elsevier, 2018, 461, pp.84-100. 10.1016/j.fluid.2017.12.036 . hal-01701205

HAL Id: hal-01701205

<https://hal-mines-paristech.archives-ouvertes.fr/hal-01701205>

Submitted on 5 Feb 2018

HAL is a multi-disciplinary open access archive for the deposit and dissemination of scientific research documents, whether they are published or not. The documents may come from teaching and research institutions in France or abroad, or from public or private research centers.

L'archive ouverte pluridisciplinaire **HAL**, est destinée au dépôt et à la diffusion de documents scientifiques de niveau recherche, publiés ou non, émanant des établissements d'enseignement et de recherche français ou étrangers, des laboratoires publics ou privés.

Thermodynamic study of binary systems containing sulphur dioxide and nitric oxide: measurements and modelling.

Benoit Creton*, Carlos Nieto-Draghi, Theodorus de Bruin,

IFP Energies nouvelles, 1 et 4 avenue de Bois-Préau, 92852 Reuil-Malmaison, France.

Véronique Lachet

*IFP Energies nouvelles, 1 et 4 avenue de Bois-Préau, 92852 Reuil-Malmaison, France.
Laboratoire de Chimie Physique, Université Paris-Sud, UMR 8000 CNRS, Orsay, France.*

Elise El Ahmar, Alain Valtz, Christophe Coquelet,

*MINES ParisTech, PSL - Research University, CTP - Centre Thermodynamique des
Procédés, 35 rue Saint Honoré, 77300 Fontainebleau, France.*

Silvia Lasala, Romain Privat, Jean-Noël Jaubert

*Université de Lorraine, Ecole Nationale Supérieure des Industries Chimiques, Laboratoire
Réactions et Génie des Procédés (UMR CNRS 7274), 1 rue Grandville, 54000 Nancy,
France.*

Abstract

In this study, the thermodynamic behaviour of NO + SO₂ mixtures has been investigated by means of molecular simulation, experiment and equation of state modelling. Quantum chemical calculation were performed to investigate possible chemical reactions between NO and SO₂. Molecular simulations were based on Monte Carlo and Molecular Dynamics techniques using force fields available in the literature. Validation of simulated vapour liquid data for NO + SO₂ binary mixtures was performed on the basis of proposed new experimental data, and new sets of parameters were optimized for the PPR78 EoS. We then moved our focus on the solubility of some gases (SO_x, NO_x, CO₂, O₂, N₂) in water and brines studied by molecular simulations. We first compared performances of some combinations of salt and water intermolecular potentials in terms of

*Corresponding author: benoit.creton@ifpen.fr

density and osmotic pressure predictions. We then studied the evolution of Henry constant values for gases in brines considering various salt concentrations and temperatures.

Keywords:

Sulphur dioxide, Nitric oxide, Brine, Molecular simulation, Experiment, EoS modelling

SYMBOLS AND ACRONYMS

$\gamma\text{-}\phi$	Activity-fugacity
BE	Bonding energy
CCS	Carbon Dioxide Capture and Storage
CoM	Centre of mass
E_{elec}	Electronic energy
EoS	Equation of State
EPM2	Rescaled Elementary Physical Model
f	Fugacity
GC	Gas Chromatograph
GHGs	Greenhouse Gases
HMCMD	Hybrid Monte Carlo Molecular Dynamics
IRC	Intrinsic Reaction Coordinate
K_H	Henry constant
k_{ij}	Binary interaction parameters
K_S	Sechenov constant
LJ	Lennard-Jones
m	Molality
MAE	Mean Absolute Error
MC	Monte Carlo
MD	Molecular Dynamics
N	Number of particles
NpT	Isobaric-isothermal ensemble
P	Pressure
PR	Peng-Robinson
p^{sat}	Vapour pressure
RMS	Root Mean Square
SPC/E	Extended Simple Point Charge
T	Temperature
TCD	Thermal conductivity detector
TIP4P/2005	Transferable Intermolecular Potential with 4 sites
U_{disp}	Dispersion interactions
U_{elec}	Electrostatic energy
U_{rep}	Repulsion interactions
VL	Vapour liquid
ZPE	Zero-point energy

1. Introduction

Facing the problem of global warming, many industrialized countries recently agreed in reducing their greenhouse gases (GHGs) emissions [1]. Industrial activities involving the combustion of fossil resources are responsible for a large part of the human induced carbon dioxide (CO₂) emissions. Various options have been already proven technically feasible to regulate anthropogenic CO₂ emissions to the atmosphere, and among them the carbon dioxide capture and storage (CCS) appears as a transitional key technology [2]. CO₂ can be stored in depleted geological reservoirs or deep saline aquifers [3, 4, 5]. Due to its origin and despite performed treatments, the injected CO₂ stream may contain small amounts of associated gaseous components such as O₂, N₂, SO_x, NO_x, as well as traces of noble gases [5, 6]. Varying amounts of such gas impurities in the CO₂ stream may induce more or less pronounced changes of the gas mixture properties, thus impacting the design and operation of CCS industrial units [6, 7, 8, 9]. Additionally, CO₂ and associated gases may react with subsurface components (brine, reservoir rocks, cap-rocks. . .) under certain salinity values, temperature and pressure conditions, affecting the long-term behaviour of the CO₂ containing mixture injected within storage sites.

The use of reactive-transport codes to investigate various scenarios is of utmost interest [10, 11, 12]. In most of the geochemical codes, chemical reactions and their equilibria are related to classical mass action laws, and water-gas equilibria are generally treated using a dissymmetrical approach $\gamma\text{-}\phi$ (*i.e.*, activity-fugacity) wherein the Henry constant (K_H) of gas species is a key property. Note that these calculations involve the use of an equation of state (EoS), and the Peng-Robinson (PR) EoS is usually used in geochemical codes [13]. EoS settings, more precisely binary interaction parameters (k_{ij}), are determined from regressions on available experimental data. The precise knowledge of the thermodynamics behaviour for binary mixtures containing: (i) CO₂ and impurities (ii) and impurities with one another, in CCS operation conditions – temperatures ranging from 218 K to 423 K and pressures up to 50 MPa [14], is necessary

31 to make accurate predictions using reactive-transport codes. Recent literature
32 reviews have highlighted a wide disparity in the experimental knowledge for such
33 binary gas mixtures [14, 15, 16, 17]. For instance, binary systems containing
34 CO₂ and oxygen (O₂) have been largely studied while there is only scarce in-
35 formation on binary systems containing sulphur dioxide (SO₂) and nitric oxide
36 (NO).

37 Molecular simulation techniques have been proven as cost-efficient alter-
38 natives to experimental measurements, especially when hazardous compounds
39 and/or extreme pressure or temperature conditions are considered. These last
40 years, we have devoted much effort to the use of molecular simulation techniques
41 to predict vapour-liquid (VL) equilibria and transport properties for binary mix-
42 tures containing CO₂ and impurities and impurities with one another, within
43 the different CCS stages [6, 7, 17, 18, 19, 20, 21]. Lachet *et al.* and Creton
44 *et al.* have generated using Monte Carlo (MC) molecular simulations, data for
45 CO₂ + SO₂ binary mixtures for temperatures ranging from 263 K to 333 K
46 and pressures up to 9 MPa [6, 19]. Lachet *et al.* and Bourasseau *et al.* have
47 studied using Gibbs ensemble MC coupled with the reactive ensemble, the be-
48 haviour of CO₂ + NO_x mixtures [18, 21]. Simulated data were obtained for
49 CO₂ + N₂O binary mixtures and CO₂ + NO binary mixtures for temperatures
50 ranging from 253 K to 293 K and pressures up to 11 MPa, and considering the
51 chemical equilibrium $2\text{NO} \rightleftharpoons \text{N}_2\text{O}_2$ [21]. Authors have demonstrated that for
52 CCS operation conditions of temperatures, only the monomer (NO) form exists.
53 Bourasseau *et al.* have studied the CO₂ + NO₂/N₂O₄ reacting system consider-
54 ing the equilibrium $2\text{NO}_2 \rightleftharpoons \text{N}_2\text{O}_4$, for temperatures ranging from 300 K to 330
55 K and pressures up to 7 MPa [18]. Some simulated data were also proposed for
56 CO₂ + Ar binary mixtures for temperatures ranging from 248 K to 288 K and
57 pressures up to 13 MPa [6]. Creton *et al.* also reported simulated data for (i)
58 CO₂ + O₂ binary mixtures for temperatures ranging from 233 K to 273 K and
59 pressures up to 12 MPa, (ii) and CO₂ + N₂ binary mixtures for temperatures
60 ranging from 220 K to 273 K and pressures up to 17 MPa [6]. Simulated phase
61 envelopes have been also proposed for binary systems of impurities with one

62 another, and El Ahmar *et al.* studied $\text{SO}_2 + \text{N}_2$ binary mixtures and $\text{SO}_2 + \text{O}_2$
63 binary mixtures for temperatures ranging from 323 K to 413 K and pressures
64 up to 85 MPa [20].

65 In the present work, we first propose new insights for $\text{SO}_2 + \text{NO}$ binary
66 systems by means of experimental and molecular simulation techniques. After-
67 wards, settings of an EoS are optimized on the basis of VL equilibrium data.
68 New experimental VL equilibrium data are proposed and compared to data ob-
69 tained with Monte Carlo molecular simulations for temperatures ranging from
70 273 K to 345 K. Generated MC simulation data are used to optimize sets of
71 parameters for a PR based EoS. We then propose a comparison of various com-
72 binations of intermolecular potentials to mimic brines behaviour using molecular
73 simulation, and provide some simulated Henry constant values in water and in
74 brines for a series of gases including SO_2 and NO .

75 **2. Materials and methods**

76 *2.1. Materials, apparatus and experimental procedure*

77 Sulphur dioxide (SO_2 , CAS number: 7446-09-5) and nitric oxide (NO , CAS
78 number: 10102-43-9) were supplied by Air Liquide with a certified purity higher
79 than 99.9 vol% and 99 vol%, respectively (Table 1). No additional purification
80 was performed before use, except for careful degassing.

81 The apparatus was designed based on a “static-analytic method” and is
82 similar to the one previously used for measurements of equilibrium properties of
83 $\text{CO}_2 + \text{NO}$ mixtures [22]. Two capillary ROLSI[®] samplers (Armines patents)
84 [23] are available to sample liquid and vapour phases. The cell volume is about
85 30 ml and it can be operated up to 473 K. The equilibrium cell is made of a
86 sapphire (aluminium oxide Al_2O_3) tube (maximum pressure 10 MPa) between
87 two Hastelloy flanges. With the sapphire tube, we have the possibility to see
88 the mixture at equilibrium conditions. A magnetic Hastelloy stirrer driven by
89 an adjustable speed external system is placed inside the cell in order to speed
90 up the reaching of the thermodynamic equilibrium.

Table 1: Chemical sample. GC stands for gas chromatograph.

Chemical name	CAS number	Source	Initial purity (weight %)	Analysis method
Sulphur dioxide	7446-09-5	Air Liquid	≥ 99.9	GC
Nitric oxide	10102-43-9	Air Liquid	≥ 99	GC

91 The sapphire cell is totally immersed in a liquid bath which keeps the tem-
 92 perature stable to ± 0.1 K. The cell is equipped with two platinum probes in
 93 order to obtain a precise measure of the temperature (± 0.02 K). The pressure
 94 in the cell is measured by a pressure transducer with an accuracy of $\pm 6.10^{-4}$
 95 MPa. The pressure transducer and temperature probes are connected to a HP
 96 data acquisition unit (HP34970A). The HP data acquisition unit is connected to
 97 a computer through a RS232 interface. The sample extracted from the cell are
 98 sent to a gas chromatograph (GC) for compositional analysis. The used GC is
 99 the Shimadzu GC-2014 equipped with a thermal conductivity detector (TCD),
 100 which is calibrated for the studied compounds. The calibration of the TCD
 101 is made by introducing known pure component volumes with appropriate GC
 102 syringes. Accuracies regarding mole numbers are $\pm 1\%$ for NO and $\pm 0.8\%$ for
 103 SO₂. The maximum standard uncertainty on liquid and vapour mole fractions
 104 ($U_{\max}(x,y)$) is 0.004. The HayeSep D (80/100 mesh 2m X 1/8" silcosteel tube)
 105 GC packed column is used.

106 2.2. Classical thermodynamics modelling

107 One of the objectives of this paper is to derive a thermodynamic model
 108 able to accurately correlate the VL equilibrium data acquired in this study.
 109 On account of its simplicity and accurateness, it was decided to use the Peng-
 110 Robinson equation of state with advanced mixing rules that combine the EoS
 111 with the residual part of an excess Helmholtz energy model, $a_{res}^{E,\gamma}$. For a mixture
 112 containing NC components with known mole fractions z_i , such mixing rules

113 write as follows [24, 25, 26]

$$\begin{cases} b_m = \sum_{i=1}^{NC} \sum_{j=1}^{NC} z_i z_j b_{ij}, \text{ with } b_{ij} = \left(\frac{b_i^{1/s} + b_j^{1/s}}{2} \right)^s \\ \frac{a_m}{b_m} = \sum_{i=1}^{NC} z_i \frac{a_i}{b_i} + \frac{a_{res}^{E,\gamma}}{\Lambda} \end{cases} \quad (1)$$

114 As a general rule, exponent s is set to a value lower or equal to 2. Parameter
 115 Λ is a constant, and its value depends on the selected cubic EoS. The pure-
 116 component parameters a_i and b_i are classically estimated from PR EoS by:

$$\begin{cases} X = \left[1 + \sqrt[3]{4 - 2\sqrt{2}} + \sqrt[3]{4 + 2\sqrt{2}} \right]^{-1} \approx 0.25308 \\ b_i = \Omega_b \frac{RT_{c,i}}{P_{c,i}}, \text{ with } \Omega_b = \frac{X}{X+3} \approx 0.077796 \\ a_i(T) = a_{c,i} \cdot \alpha_i(T), \text{ with:} \\ a_{c,i} = \Omega_a \frac{R^2 T_{c,i}^2}{P_{c,i}}, \text{ and } \Omega_a = \frac{8(5X+1)}{49-37X} \approx 0.45723 \\ \alpha_i(T) = \left[1 + (0.37464 + 1.54226\omega_i - 0.26992\omega_i^2) \left(1 - \sqrt{\frac{T}{T_{c,i}}} \right) \right]^2 \end{cases} \quad (2)$$

117 The Soave α -function incorporated in the original PR EoS model has been
 118 maintained as it retains a thermodynamically consistent behavior [27, 28, 29]
 119 in the whole temperature domain of interest for the two considered compo-
 120 nents (up to about 600 K for NO and 2000 K for SO₂). The PR EoS was not
 121 volume-translated [30, 31] since such a translation does not affect VL equilib-
 122 rium calculations.

123 Following our previous studies on binary systems involved in CCS processes
 124 [16, 32], it was first decided to correlate the available data with the PPR78
 125 model [33, 34]. For such a model, exponent s in equation (1) must be set to
 126 unity and the activity coefficient model ($a^{E,\gamma}$) is a one-parameter Van Laar
 127 expression:

$$\frac{a_{res}^{E,\gamma}}{\Lambda} = \frac{1}{2} \cdot \frac{\sum_{i=1}^{NC} \sum_{j=1}^{NC} z_i z_j b_i b_j E_{ij}(T)}{\sum_{i=1}^{NC} z_i b_i} \quad (3)$$

128 As required by equation (1), such an expression is a purely residual a^E model
129 (it does not contain a combinatorial part). Following the mixing rule derived
130 for the PPR78 model, the unique E_{12} parameter in equation (3) – needed to
131 correlate the phase behavior of the NO + SO₂ binary system – was selected
132 temperature-dependent through the following relation:

$$E_{12} = A_{12} \cdot \left(\frac{298.15}{T} \right)^{\left(\frac{B_{12}}{A_{12}} - 1 \right)}, \quad (4)$$

133 where A_{12} and B_{12} are two adjustable parameters. In order to improve the
134 quality of the correlation, the Van Laar a^E model was subsequently replaced
135 by the more sophisticated Wilson model. This second study was conducted
136 because the NO + SO₂ mixture exhibits a type III phase behaviour and that
137 such systems are known to be particularly difficult to correlate.

138 *2.3. Molecular simulation techniques*

139 The GIBBS Monte Carlo code [35] has been used to generate thermody-
140 namic data for studied systems containing gaseous components and/or water
141 and/or salts. VL equilibrium data were obtained with MC molecular simula-
142 tions performed in the Gibbs NpT – isobaric-isothermal – ensemble where the
143 number of particles (N), the total pressure (P) and the temperature (T) are
144 constant [36, 37]. During these MC simulations, vapour and liquid phases are
145 simultaneously considered in two distinct simulation boxes, without considering
146 their interface. Transfers of particles between the two simulation boxes ensure
147 the chemical equilibrium of the system. The sampling of the configurational
148 space is ensured by different Monte Carlo moves, such as rigid body transla-
149 tions or rotations of molecules, and volume changes. The used MC moves and
150 associated attempt probabilities are as follows: rigid body translations (0.2975),
151 rotations (0.2975), volume changes (0.0050), and transfers (0.4000). For trans-
152 lation, rotation, and volume change moves, maximum amplitudes were adapted
153 to reach acceptance rates of 0.4. The studied systems contained in between 1000
154 and 2000 molecules depending on the vicinity of the critical point. For each MC

155 simulation, the number of generated configurations ranged within 2.10^8 and
156 2.10^9 including the equilibration of the system and the production run.

157 In the case of strongly associated systems such as brines, the above men-
158 tioned MC moves are not efficient enough to sample the configurational part
159 of the phase space, and reaching the equilibrium state may necessitate impor-
160 tant computational resources. To improve the sampling efficiency, we performed
161 Hybrid Monte Carlo Molecular Dynamics (HMCMD) simulations [38, 39]. An
162 HMCMD move consists in letting the system evolves deterministically through
163 the phase space using a short Molecular Dynamics (MD) run as a MC move,
164 in addition to other usual moves. In contrast to MC simulations, MD simula-
165 tions enable the exploration of the whole phase space (*i.e.* all possible values
166 of positions and momenta) with collective motions of all particles at each time
167 step. MD steps were performed using the NEWTON Molecular Dynamics code
168 developed for flexible and rigid molecules [40]. Hereafter, a HMCMD move cor-
169 responds to 50 MD steps with an adjustable MD time step so as to reach an av-
170 erage acceptance ratio of *ca.* 40%. All details regarding the implementation and
171 the combination of the GIBBS and NEWTON codes are given elsewhere [39].

172 Molecular Dynamics simulations were performed with the NEWTON code
173 to generate osmotic pressure values following the method proposed by Luo and
174 Roux [41]. It consists in introducing virtual walls in the simulation box to sep-
175 arate brine and pure water regions, only water molecules can move from one
176 region to the other. Forces resulting from interactions of ions with the walls
177 are handled by a harmonic potential (with a constant of $41.9 \text{ kJ.mol}^{-1}.\text{\AA}^{-2}$).
178 The walls are placed with a separation distance in agreement with the desired
179 ionic concentration. Ions leaving the constraint zone feel a force in the oppo-
180 site direction (normal to the wall) in order to maintain them inside the ionic
181 region (between the walls). The total average force exerted by the ions to the
182 walls is directly related to the osmotic pressure. MD simulations start with an
183 equilibration period where the system is relaxed by means of a 1 ns run using
184 the NPzzT ensemble ($P_{zz} = 0.1 \text{ MPa}$ and $T = 298.15 \text{ K}$), relaxing the size
185 of the simulation box in the z direction. During this equilibration period, the

186 distance between walls is fixed in order to preserve the volume occupy by ions
187 (i.e. the ionic concentration of the system). After this period the average box
188 size in z direction is computed and the average Lz value is imposed to the sys-
189 tem. Then, an additional 2 ns equilibrium simulation in the NVT ensemble (T
190 = 298 K) is performed and followed by a 5 ns production run. Three different
191 simulation runs, starting from independent initial configurations, were used to
192 produce average values of the osmotic pressure for each system. The orthorhom-
193 bic simulation boxes are composed of about 3000 water molecules divided into
194 two regions: one contains the brine and the other contains pure water, with the
195 pure water region representing two thirds along the z-axis.

196 *2.4. Molecular models and force fields*

197 As described hereafter, only rigid body molecules are considered thus no in-
198 tramolecular energy has been computed. The total potential energy of the sys-
199 tems is calculated as the sum of the two contributions: dispersion-repulsion in-
200 teractions (U_{disp} and U_{rep}) and the electrostatic energy (U_{elec}). A 12-6 Lennard-
201 Jones (LJ) potential (equation (5)) has been used to represent the dispersion-
202 repulsion energy between two force centres i and j belonging to different molecules
203 and separated by a distance r_{ij} . During MC and MD simulations, U_{ij} interac-
204 tions were evaluated using a spherical cut-off radius equal to half the size of the
205 cubic simulation box, associated with standard long-range corrections.

$$U_{ij} = U_{rep} + U_{disp} = 4\epsilon_{ij} \left(\left(\frac{\sigma_{ij}}{r_{ij}} \right)^{12} - \left(\frac{\sigma_{ij}}{r_{ij}} \right)^6 \right), \quad (5)$$

206 where ϵ_{ij} and σ_{ij} are the LJ parameters, and equations (6) and (7) present the
207 Lorentz-Berthelot combining rules used to compute cross interaction parame-
208 ters.

$$\epsilon_{ij} = \sqrt{\epsilon_i \epsilon_j}, \quad (6)$$

$$\sigma_{ij} = \frac{\sigma_i + \sigma_j}{2}. \quad (7)$$

209 During both MC and MD simulations, U_{elec} was computed from the Coulomb
210 law (equation (8)) and evaluated using the Ewald summation method with 7
211 vectors in each direction of the space and a gaussian width set to $2\pi/L$, where
212 L is the length of the cubic simulation box.

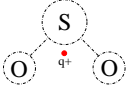


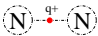
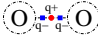
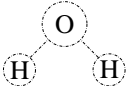
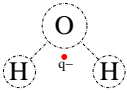
$$U_{elec} = \frac{1}{4\pi\epsilon_0} \frac{q_i q_j}{r_{ij}}, \quad (8)$$

213 where q_i and q_j are two point charges belonging to different molecules and
214 spaced by r_{ij} , and ϵ_0 is the vacuum permittivity.

215 Values of ϵ_i , σ_i , and q_i parameters constitute the force field parameters. The
216 GIBBS MC and the NEWTON MD simulation codes have both already been
217 successfully used with intermolecular potentials listed in Table 2, and calcula-
218 tions have already shown good accuracy in the restitution of both equilibrium
219 and/or transport properties for pure SO₂, NO, CO₂, N₂, and O₂ as well as some
220 mixtures of these gases [6, 20, 21].

221 Force field parameters used to mimic SO₂, NO, CO₂, N₂, and O₂ are sum-
222 marized in Table 2. The model developed by El Ahmar *et al.* has been used to
223 mimic properties of sulphur dioxide [20]. The SO₂ molecule is represented as
224 follows: each atom of the molecule is a LJ centre, and the S–O distance and
225 the $\widehat{\text{OSO}}$ angle are equal to 1.434 Å and 119.50°, respectively. A negative point
226 charge is located on each oxygen atoms, and q^+ a positive point charge is placed
227 on the bisector of the $\widehat{\text{OSO}}$ angle at 0.312 Å from the sulphur atom, as illustrated
228 in Table 2. The force field chosen to reconstitute molecular nitric oxide behavior
229 was developed by Lachet *et al.* [21]. It consists of a single Lennard-Jones sphere.
230 Note that this model well reproduces the variation of mole fraction of associated
231 N₂O₂ as a function of temperature along the saturation line for the bulk liquid
232 phase of the 2NO \rightleftharpoons N₂O₂ system. The carbon dioxide has been extensively
233 studied using molecular simulations, and the rigid version of the rescaled ele-
234 mentary physical model (EPM2) proposed by Harris and Yung [42] has shown
235 that VL equilibrium data for pure CO₂ are well reproduced. Each atom carries
236 both a LJ centres and an electrostatic point charge, and the C–O distance is

Table 2: Force field parameters for the studied molecules.

Molecule	Force centre or charge	$\sigma(\text{\AA})$	$\epsilon(\text{K})$	$q(e)$	Ref.
	S	3.5830	126.0800	—	[20]
	O	2.9900	46.4100	-0.4140	
	q^+	—	—	0.8280	
	NO	3.4000	130.0000	—	[21]
	O	3.0330	80.5070	-0.3256	[42]
	C	2.7570	28.1290	0.6512	
	N	3.3000	36.0000	-0.5075	[43]
	q^+	—	—	1.0150	
	O	3.1062	43.1830	—	[44, 45]
	q^-	—	—	-2.1000	
	q^+	—	—	4.2000	
	O	3.1655	78.1974	-0.8476	[46]
	H	—	—	0.4238	
	O	3.1589	93.1990	—	[47]
	H	—	—	0.5564	
	q^-	—	—	-1.1128	

237 equal to 1.149 Å. It is important to mention that although the model has been
238 developed using geometric combining rules, Nieto-Draghi *et al.* have shown that
239 the combination of the EPM2 force field parameters with the Lorentz-Berthelot
240 rules allows a good restitution of both thermodynamic and transport proper-
241 ties [48]. The molecular nitrogen has been represented using the force field
242 developed by Delhommelle [43]. The two N atoms are separated by 1.098 Å
243 and each of them carries a LJ centre and a negative charge, a positive charge is
244 placed on the centre of mass (CoM) of the molecule. On the basis of previous
245 works, we have decided to mimic the oxygen behaviour using the Boutard *et*
246 *al.* adaptation [45] of the Vrabc potential [44]. The two oxygen atoms carry
247 each a LJ centre, and are separated by 1.210 Å. A positive electrostatic charge
248 is located in between the two O atoms, and two negative charges are placed at
249 0.200 Å on both sides of the CoM of the molecule along the O–O bond.

250 Numerous potentials have been developed to mimic water properties with
251 varied associated performances [49]. Among existing, we chose two widespread
252 used models: the extended simple point charge (SPC/E) [46] and the trans-
253 ferable intermolecular potential with 4 sites (TIP4P/2005) [47], being aware of
254 limitations of models involving rigid geometries and fixed electrostatic charges
255 (*i.e.*, non-polarizable models) [50, 51]. In the two selected models water is con-
256 sidered as a rigid body molecule, the oxygen atom of the molecule is a LJ centre
257 and hydrogen atoms carry positive charges. The $\widehat{\text{HOH}}$ angle is 109.47° and
258 104.52° for the SPC/E and TIP4P/2005 models, respectively. For the SPC/E
259 model, a negative point charge is placed on the oxygen atom and the O–H
260 bond length is 1.000 Å. For the TIP4P/2005 model, a negative point charge is
261 placed on the bisector of the $\widehat{\text{HOH}}$ angle at 0.1546 Å from the oxygen atom,
262 and the O–H bond length is 0.9572 Å. All details regarding force field parame-
263 ters are summarized in Table 2. Sakamaki *et al.* compared performances of 12
264 non-polarizable water models including the SPC/E and TIP4P/2005 models to
265 calculate, among others properties, VL equilibrium densities for temperatures
266 from about 200 K to 650 K [52]. Recently, Vinš *et al.* performed a similar study
267 focusing on the SPC/E and TIP4P/2005 models [53]. In this latter work, au-

Table 3: Force field parameters considered for the sodium and chloride ions: OPLS, Whee, GoS, GoT, and Aqv refer to the parameter set proposed by Jorgensen *et al.*, the parameter set proposed by Wheeler and Newman, the parameter set proposed by Goo *et al.* in combination with SPC/E, the parameter set proposed by Goo *et al.* in combination with TIP4P/2005, and the parameter set proposed by Åqvist, respectively.

Label	Ion	LJ centre		Ref.
		$\sigma(\text{\AA})$	$\epsilon(\text{K})$	
OPLS	Na ⁺	1.8974	808.7	[54, 55]
	Cl ⁻	4.4172	59.3	
Whee	Na ⁺	2.3500	55.3	[56]
	Cl ⁻	4.4200	54.2	
GoS	Na ⁺	2.5864	50.3	[57]
	Cl ⁻	4.4044	50.3	
GoT	Na ⁺	2.5931	42.2	
	Cl ⁻	4.4111	42.2	
Aqv	Na ⁺	3.3304	1.4	[54, 55, 58]
	Cl ⁻	4.4172	59.3	

268 thors reported the following absolute deviations from experimental data: (i) at
 269 250 K, 0.6% and 0.2% for the SPC/E and TIP4P/2005 models, respectively (ii)
 270 and at 500 K, 5.3% and 1.9% for the SPC/E and TIP4P/2005 models, respec-
 271 tively. We performed similar simulations and our results agreed with previous
 272 observations.

273 We have considered five sets of parameters for the sodium (Na⁺) and chlo-
 274 ride (Cl⁻) ions in which both of them are represented as a sole LJ sphere with
 275 an associated positive (+1|e|) charge and negative (-1|e|) charge, respectively.
 276 Force field parameters used to mimic the sodium (Na⁺) and chloride (Cl⁻) ions
 277 are summarized in Table 3. Neyt *et al.* have computed densities for NaCl aque-
 278 ous solutions at 298 K and 0.1 MPa covering molalities up to 5.5 mol.kg⁻¹, and
 279 demonstrated that the combination OPLS with TIP4P/2005 performs better
 280 than others such as Reif [59] with TIP4P/2005 [60, 61]. Orozco *et al.* compared
 281 some salt models combined with SPC/E based water potentials for tempera-

Table 4: Force field parameters considered for the calcium and chloride ions: Matt, GoS, GoT, Pred, and Aqv refer to the parameter set proposed by Matthews *et al.* and Jorgensen *et al.*, the parameter set proposed by Goo *et al.* in combination with SPC/E, the parameter set proposed by Goo *et al.* in combination with TIP4P/2005, the parameter set proposed by Předota *et al.*, and the parameter set proposed by Åqvist, respectively.

Labels	Ions	LJ centre		Ref.
		$\sigma(\text{Å})$	$\epsilon(\text{K})$	
Matt	Ca ²⁺	2.7101	15.1	[54, 55, 64]
	Cl ⁻	4.4172	59.3	
GoS	Ca ²⁺	1.5944	85.6	[57, 65]
	Cl ⁻	4.4044	50.3	
GoT	Ca ²⁺	1.6011	71.8	
	Cl ⁻	4.4111	42.2	
Pred	Ca ²⁺	2.8950	50.3	[66, 67]
	Cl ⁻	4.4010	50.3	
Aqv	Ca ²⁺	2.4120	226.3	[54, 55, 58]
	Cl ⁻	4.4172	59.3	

282 tures and pressures up to 473 K and 1000 bar, respectively [62].
283 Five sets of parameters have been considered to describe calcium (Ca²⁺) and
284 chloride (Cl⁻) ions in which both of them are represented as a sole LJ sphere
285 with an associated positive (+2|e|) charge and negative (-1|e|) charge, respec-
286 tively. Force field parameters used to mimic the calcium (Ca²⁺) and chloride
287 (Cl⁻) ions are summarized in Table 4. Note that Tsai *et al.* recently compared
288 three sets of parameters including GoS and Aqv using two point charge based
289 models (SPC and SPC/E) for water [63]. Performed comparisons have revealed
290 that among the 6 considered combinations for water – CaCl₂ models, SPC/E
291 – Aqv gives the best density predictions at 373 and 473 K with, nevertheless,
292 a significant underestimation of experimental densities at 373 and 473 K.

293 2.5. Electronic structure calculations

294 The electronic structure calculations were performed with the Gaussian 09
295 suite of programs [68]. All geometry optimizations were performed with the hy-

296 brid M06 functional [69] using the spin unrestricted formalism (uM06), in com-
297 bination with the 6-311+G(d,p) basis set. Systematic conformational searches
298 were performed to identify the most stable structures. Standard convergence
299 criteria were applied, *i.e.* 1×10^{-8} Hartree for the electronic energy convergence,
300 while for the geometry, convergences of 0.00045 and 0.00030 Hartree/Bohr for
301 respectively the maximum and root mean square (RMS) forces were used, and
302 threshold values of 0.0018 and 0.0012 Bohr for the maximum and RMS dis-
303 placements, respectively. The character of the localized stationary points, *i.e.*
304 minimum or first order transition state, on the potential energy surface was
305 determined by calculating the Hessian matrix (2^{nd} derivative of the energy with
306 respect to the atomic displacements). Furthermore, using intrinsic reaction
307 coordinate (IRC) calculations it was verified that the transition state indeed
308 connects reactants and products. Thermodynamic (enthalpic and entropic)
309 contributions were calculated with the use of the partition functions within
310 the harmonic oscillator and the perfect gaz approximation. Additionally, the
311 resulting calculated vibrational frequencies have not been adjusted with an em-
312 pirical correction factor. After the desired character of the stationary point was
313 confirmed, the electronic wavefunction was subjected to a stability analysis to
314 verify the presence of any singlet/triplet or doublet/quartet instabilities.

315 In this study, the uM06 functional in combination with the 6-311+G(d,p)
316 basis set was selected, since it reproduces reasonably well the electronic state
317 of the NO dimer. The NO dimer seems best described using a multi-reference
318 method together with a large basis set [70], however, these methods can quickly
319 become prohibitive for the systems investigated in this study, with respect to
320 the needed computer resources.

321 **3. Results and discussion**

322 In this section, we present a series of new VL experimental data, together
323 with modelling data obtained using both EoS and molecular simulation tools.
324 We investigate NO + SO₂ systems using the three above mentioned techniques

325 (experimental, EoS, molecular simulations). Concerning molecular simulation
326 we first studied chemical reactions that may occur in the gas phase and we then
327 generate simulated vapour liquid equilibrium data for a broad range of temper-
328 atures. We then move our focus on the solubility of different gases (CO_2 and
329 associated gases such as O_2 , N_2 , SO_x , NO_x) in brines. For this second study,
330 simulation results are divided into two main parts devoted to the study of the
331 solubility in water and in brines, respectively. The solubility is first expressed
332 in terms of Henry constant values. In the case of sulphur dioxide solubility in
333 water, we characterize deviations to the Henry’s law with increasing pressure
334 conditions. A similar solubility study is then proposed in the case of brines con-
335 taining NaCl or CaCl_2 . We present a comparison of some combinations of salt
336 and water potentials in terms of density and osmotic pressure predictions. We
337 propose the generation of simulated Henry constant values for CO_2 , SO_2 , NO ,
338 O_2 , and N_2 in brines considering various salt concentrations and temperatures.

339 3.1. Investigation of chemical reactions within $\text{NO} + \text{SO}_2$ systems

340 Before studying phase equilibrium in $\text{NO} + \text{SO}_2$ systems, we first investigate
341 the stability of such mixtures by means of electronic structure calculations. Such
342 calculations have been performed in the gas phase, considering the following
343 chemical reaction: $\text{SO}_2 + 2 \text{NO} \rightleftharpoons \text{SO}_3 + \text{N}_2\text{O}$. With the use of the applied
344 method (see section 2.5) the singlet spin 1A_1 is calculated to be slightly more
345 stable than the 3B_2 triplet state by $0.99 \text{ kcal.mol}^{-1}$, which is in accordance with
346 the CASSCF results of Sayos *et al.* [71], see Table 5. However, it appears that
347 the calculated singlet electronic structure has an instability, while the triplet
348 state is stable under the considered perturbations. We therefore have taken the
349 triplet state as the most stable electronic configuration. All other calculated
350 species have a singlet electronic ground state, except for NO , where the doublet
351 spin state is largely more stable than the quartet spin state ($>123 \text{ kcal.mol}^{-1}$).

352 The here applied method correctly reproduces the dimer dissociation energy
353 (probably as a result of a fortunate cancellation of errors). Yet, the bond dis-
354 tances are slightly less well reproduced. Since we are mostly interested in the

energetics in this study, we consider this of smaller importance.

Figure 1 shows the energy reaction profile for the $\text{SO}_2 + 2 \text{NO}$ reaction to yield SO_3 and N_2O for the electronic energy corrected for the zero-point energies (ZPE), the enthalpy changes at 298 K and the Gibbs energy at 298 K and 0.1 MPa. Starting with the reactants, 2 NO and SO_2 (**M0**), first the *cis* NO dimer is formed with the SO_2 molecule at infinite distance (**M1**). Then the system goes through a transition state, where one NO molecule is nearly 90 degrees rotated and the $\widehat{\text{ONNO}}$ dihedral angle changes from 0.0 in **M1** to -84.3 degrees in **T1**. Next, the NO molecule continues its rotation to obtain a geometry where the two NO molecules are again in the same plane (**M2**). However, this configuration now more corresponds to the *trans* dimer, where one of the two molecules is shifted. Next, the transition takes place in which an oxygen atom is transferred from one NO molecule to the SO_2 molecule. This transition state (**T2**) is characterized by an imaginary frequency of $i745.1 \text{ cm}^{-1}$ and a NO distance of 1.433 Å in **T1** (1.147 Å in **M2**).

The very small energy barrier for the $\text{M1} \rightleftharpoons \text{T1} \rightleftharpoons \text{M2}$ transition indicates a rapid *cis/trans* isomerization, while the significantly larger energy barrier for the $\text{M2} \rightleftharpoons \text{T2} \rightleftharpoons \text{M3}$ transition corresponds to the rate determining step of the overall reaction.

Upon considering the three energy profiles in Figure 1 it is seen that all three clearly show that the overall reaction is thermodynamically favored. The thermal corrections ($T = 0 \text{ K}$ to $T = 298 \text{ K}$) only have a minor impact on the relative stabilities of the different species, whereas the entropy significantly destabilizes both the transition state **T2** and the final products **M3**. As can be seen from Figure 2, the entropy (or more precisely the $T\Delta S$ term) becomes smaller during the course of the reaction with an overall minimum for **T2**, where the three reactants essentially form one single species. An increase of the temperature, *e.g.* from 273 to 345 K, has an endergonic contribution to the Gibbs energy, while a pressure increase from 0.1 to 5.0 MPa yields an exergonic contribution to ΔG .

From Table 6 it is seen that the reaction barrier (ΔG_a) that corresponds to

Table 5: Properties of the *cis* NO dimer calculated at the M06 level, using the multi-reference CASSCF method [71], and experimental data. BE, ZPE, and E_{elec} stands for bonding energy, zero-point energy, and electronic energy, respectively.

	M06/ 6-311+G(d,p)	CASSCF(18,14)/ 6-311G(2d)	Exp.
BE (kcal.mol ⁻¹)	3.27	4.31	2.18 [72]
BE + Δ ZPE (kcal.mol ⁻¹)	1.86	1.43	—
Δ E (kcal.mol ⁻¹)*	0.99	5.56	—
r(NN) (Å)	1.972	2.327	2.263 [73]
r(NO) (Å)	1.146	1.159	1.152 [73]

* $\Delta E = E_{elec}(\text{triplet}, {}^3B_2) - E_{elec}(\text{singlet}, {}^1A_1)$.

Table 6: Energy changes (kcal.mol⁻¹) of the most important transitions under different temperature and pressure conditions.

	$\Delta E + \Delta ZPE$ (0 K)	ΔH (298 K)	ΔG (298 K, 0.1MPa)	ΔG (298 K, 5MPa)	ΔG (345 K, 0.1MPa)
M0 \rightleftharpoons M1	-1.9	-2.6	5.9	3.6	7.2
M1 \rightleftharpoons T1	1.3	1.7	-0.2	-0.2	-0.4
M1 \rightleftharpoons M2	1.2	1.2	1.1	1.1	1.1
M2 \rightleftharpoons T2 (Δ_a)	33.7	32.4	46.9	44.6	49.2
M0 \rightleftharpoons M2 (Δ_R)	-39.8	-41.3	-29.0	-31.4	-27.1

386 the rate determining step (**M2** \rightleftharpoons **T2**), stays well beyond +40 kcal.mol⁻¹ in the
387 investigated temperature and pressure ranges. It can thus be concluded that, in
388 spite of the fact the reaction is thermodynamically favored (ΔG_R), the overall
389 reaction is kinetically prohibited. No chemical reaction will thus be considered
390 hereafter in the study of NO + SO₂ systems.

391 3.2. VL equilibrium for NO + SO₂ systems

392 In this section, we propose new experimental VL data (generated using the
393 apparatus described in section 2.1) for pressures up to 10 MPa. Molecular
394 simulation tools were then used to supplement VL data at higher pressures.

395 Finally, all VL data were used to optimize settings of the PPR78 EoS.

396 The apparatus described above has been used to acquire experimental data
397 for NO + SO₂ binary mixtures. In this work, only vapour phases have been
398 sampled. Experimental vapour phase compositions have been measured for the
399 NO + SO₂ binary mixtures at 273.07 K, 313.21 K, and 343.28 K, and pressures
400 up to 10 MPa. So-obtained mole fractions are reported in Table 7. Figure 3
401 plots pressures against experimental NO mole fractions for vapour phases of the
402 studied systems. New experimental data are compared with those reported by
403 Xu *et al.* [16], and both sets are consistent.

404 VL equilibrium data were obtained using MC molecular simulations per-
405 formed in the Gibbs NpT ensemble. The studied systems contained in between
406 1000 and 2000 molecules depending on the vicinity of the critical point of the
407 studied mixture. For each MC simulation, the number of generated configura-
408 tions ranged within $2 \cdot 10^8$ and $6 \cdot 10^8$ including the equilibration of the system
409 and the production run. Statistical uncertainties associated to calculated phase
410 properties were determined using the block averaging technique [74], and on
411 liquid densities they are typically 1-2%, but higher values are found at near-
412 critical temperatures as a result of larger fluctuations. Table 8 summarizes the
413 calculated VL equilibrium data. Figure 3 presents pressure plotted against liq-
414 uid and vapour phases mole fractions of NO, at 273.15, 293.15, 313.15, 324.15,
415 and 345.15 K. The considered temperatures are below the SO₂ critical tem-
416 perature (430.75 K), all phase diagrams exhibit a critical point, except that
417 obtained at 273.15 K for which molecular simulations do not indicate an obvi-
418 ous closing trend of the phase envelope. Simulated critical coordinates of NO
419 + SO₂ mixtures were estimated by extrapolating MC simulation results with
420 scaling laws, as described in equations (9) and (10), and detailed in previous
421 works [6, 19, 20, 35]. The so-obtained critical coordinates, *i.e.* the critical den-
422 sity ρ_c , the critical composition x_c , and the critical pressure P_c , are given in

Table 7: Experimental compositions of the vapour phase for NO + SO₂ binary mixtures at 273.07 K, 313.21 K, and 343.28 K. n is the number of samples, y_{NO} is the NO molar fraction in the vapour phase, and $\sigma_{y_{NO}}$ is the repeatability on vapour compositions. $U_{\max}(y)$ is 0.004, $U(P)$ is 6.10^{-4} MPa, and $U(T)$ is 0.02 K

P (MPa)	n	y_{NO}	$\sigma_{y_{NO}}$
$T = 273.07$ K			
0.4866	6	0.6580	0.0020
1.0115	16	0.8283	0.0005
2.0609	11	0.9096	0.0002
3.2926	8	0.9372	0.0001
6.1645	6	0.9551	0.0002
10.8416	5	0.9618	0.0001
$T = 313.21$ K			
1.2488	9	0.4390	0.0030
1.8063	8	0.6090	0.0020
3.2242	6	0.7570	0.0050
5.1040	5	0.8270	0.0040
9.2503	10	0.8580	0.0020
14.173	6	0.8810	0.0010
$T = 343.28$ K			
2.2584	5	0.3091	0.0060
3.5153	6	0.5190	0.0040
5.5226	7	0.6530	0.0060
7.7624	7	0.7190	0.0040
9.9743	6	0.7420	0.0090
12.7731	6	0.7530	0.0040
16.1085	4	0.7620	0.0030

423 Table 8.

$$\rho_i = \rho_c + \zeta \frac{\gamma}{2} (P_c - P)^\beta + \lambda (P_c - P), \quad (9)$$

$$x_i = x_c + \left(\lambda_1 - \zeta \frac{\lambda_2}{2} \right) (P_c - P) - \zeta \frac{\mu}{2} (P_c - P)^\beta, \quad (10)$$

424 where, $\beta = 0.325$, and $\zeta = 1$ or -1 whether it refers to the liquid or vapour
 425 phase, respectively. Parameters (γ , λ , λ_1 , λ_2 , and μ) of equations (9) and
 426 (10) are regressed from a set of simulated coexistence data (*i.e.*, (P , ρ_l , ρ_v)
 427 and (P , x_l^{NO} , x_v^{NO}), where subscripts l and v denote the liquid phase and the
 428 vapour phase, respectively). Figure 4 presents pressure plotted against liquid
 429 and vapour phase densities at 273.15, 293.15, 313.15, 324.15, and 345.15 K. To
 430 the best of our knowledge, there is no volumetric data available in the literature
 431 to compare our results with.

432 Correlation of the NO + SO₂ binary system by means of the PPR78 EoS
 433 [16] was performed by Xu *et al.* who proposed to use $A_{12} = 172.3$ MPa and
 434 $B_{12} = 1343.2$ MPa, see equation (4). Such parameters were however determined
 435 considering only six experimental data points. In this study, it was decided to
 436 refit such parameters over all the available VL equilibrium data. The following
 437 objective function (*O.F.*) was minimized:

$$O.F. = \sum_{i=1}^{n.b.} |x_i^{exp} - x_i^{calc}(T_i^{exp}, P_i^{exp})| + \sum_{i=1}^{n.d.} |y_i^{exp} - y_i^{calc}(T_i^{exp}, P_i^{exp})| \quad (11)$$

438 where, *n.b.* and *n.d.* designate the number of bubble and dew points, respec-
 439 tively. The derived optimal parameters for equation (4) – not so different from
 440 the ones obtained by Xu *et al.* [16] –, are $A_{12} = 127.6$ MPa and $B_{12} = 856.8$
 441 MPa. Figures 3 shows data points and results of calculation obtained with the
 442 PPR78 EoS model. Isothermal phase diagrams at $T = 273.15$ K, $T = 293.15$
 443 K, $T = 313.15$ K, $T = 324.15$ K, $T = 345.15$ K (Figure 3) and the global phase
 444 equilibrium diagram for the NO + SO₂ mixture (Figure 5) were calculated.

Table 8: Calculated vapour liquid equilibrium compositions and densities for the NO + SO₂ mixture at different temperatures.

T (K)	P (MPa)	x_v^{NO}	ρ_v (kg.m ⁻³)	x_l^{NO}	ρ_l (kg.m ⁻³)	T (K)	P (MPa)	x_v^{NO}	ρ_v (kg.m ⁻³)	x_l^{NO}	ρ_l (kg.m ⁻³)
273.15	0.2#	0.00000	4.6	0.00000	1440.1	313.15	0.7#	0.00000	18.7	0.00000	1332.6
	1.5	0.01142	23.4	0.87258	1435.3		1.5	0.00808	28.6	0.52200	1325.5
	3.0	0.02517	44.9	0.93108	1425.8		3.0	0.02238	48.2	0.73322	1318.2
	5.0	0.04194	75.2	0.95070	1417.4		5.0	0.04151	75.1	0.82048	1307.1
	10.0	0.07994	158.2	0.96230	1399.4		10.0	0.08840	147.2	0.87900	1281.2
	15.0	0.11936	248.3	0.96373	1378.1		15.0	0.13611	224.9	0.88985	1252.3
	20.0	0.14771	342.8	0.95719	1366.1		20.0	0.18079	307.9	0.88492	1226.7
	25.0	0.17037	430.5	0.94785	1358.5		25.0	0.22725	391.8	0.87307	1198.5
	30.0	0.19672	502.8	0.93996	1346.1		30.0	0.27163	477.7	0.85127	1171.6
	35.0	0.22173	561.0	0.93484	1334.9		35.0	0.30865	569.8	0.81457	1152.1
	40.0	0.23590	615.2	0.92370	1332.8		40.0	0.38648	665.2	0.76935	1089.9
	45.0	0.26086	657.5	0.91681	1321.4		42.7*	0.56971	907.9	0.56971	907.9
	50.0	0.28289	691.2	0.91214	1312.0	324.15	0.9#	0.00000	24.6	0.00000	1297.1
	55.0	0.30074	725.5	0.90456	1306.8		3.2	0.02213	54.4	0.65618	1286.2
	60.0	0.31492	751.9	0.90049	1304.0		5.0	0.03982	78.1	0.75245	1275.8
	65.0	0.32828	784.4	0.88859	1302.1		10.0	0.08817	149.6	0.83536	1247.6
293.15	0.3#	0.00000	9.5	0.00000	1384.9		15.0	0.13662	225.5	0.85384	1218.9
	1.5	0.01046	25.0	0.73761	1381.8		20.0	0.19058	306.6	0.85384	1183.0
	3.0	0.02371	45.3	0.85498	1375.5		25.0	0.24291	398.8	0.83357	1147.6
	5.0	0.04170	73.6	0.90118	1366.4		30.0	0.30027	490.6	0.80785	1108.1
	10.0	0.08582	149.5	0.93121	1340.9		35.0	0.37495	595.1	0.76037	1047.0
	15.0	0.12644	232.1	0.93359	1319.7		37.8*	0.57676	836.2	0.57676	836.2
	20.0	0.16297	318.6	0.92786	1300.8	345.15	1.6#	0.00000	42.1	0.00000	1232.3
	25.0	0.20117	401.6	0.91891	1279.2		3.9	0.02411	73.9	0.50703	1223.6
	30.0	0.24074	478.7	0.90658	1256.3		7.0	0.05746	113.9	0.68165	1197.1
	35.0	0.27427	544.2	0.89477	1238.9		10.0	0.09115	156.6	0.74079	1173.3
	40.0	0.30313	602.5	0.88039	1225.0		15.0	0.15237	231.7	0.77920	1128.3
	45.0	0.33635	660.4	0.86152	1208.3		20.0	0.21368	318.0	0.77616	1086.2
	50.0	0.36514	716.1	0.83725	1194.2		25.0	0.28384	420.9	0.74666	1033.5
	55.0	0.41668	819.3	0.76114	1159.0		27.0	0.31836	456.2	0.73929	1001.0
	57.7*	0.58231	1007.4	0.58231	1007.4		29.0	0.36071	508.8	0.71747	960.8
							31.3*	0.54987	744.1	0.54987	744.1

* Critical coordinates obtained using extended scaling laws, see equations (9) and (10).

Pure SO₂ liquid vapour equilibrium data obtained using GIBBS NVT MC simulations.

445 As shown by Figure 5, the NO + SO₂ mixture exhibits a type III phase be-
 446 haviour according to the classification scheme by van Konynenburg and Scott
 447 [75, 76]. The VL equilibrium data of such systems are acknowledged to be diffi-
 448 cult to correlate with an EoS, and it is thus not surprising to observe deviations
 449 between calculated and experimental data points. In particular, the use of a
 450 one-parameter a^E model, like the van Laar model, in the advanced mixing rules
 451 implemented in this study tends to strongly overestimate critical pressures pre-
 452 dicted using MC simulations. From our experience [24, 25, 26], the quality of
 453 the correlation can however be significantly improved by coupling the PR EoS
 454 with the residual part of the Wilson a^E model. For a binary system, such a
 455 model writes as follows:

$$\frac{a_{res}^{\gamma Wilson}(T, \zeta)}{RT} = -z_1 \ln \left[\Phi_1 + \Phi_2 \exp \left(-\frac{A_{12}}{RT} \right) \right] - z_2 \ln \left[\Phi_1 \exp \left(-\frac{A_{21}}{RT} \right) + \Phi_2 \right] \quad (12)$$

456 A_{12} and A_{21} are the two adjustable parameters and $\Phi_i = z_i \mathbf{v}_i / \sum_{j=1}^{NC} (z_j \mathbf{v}_j)$ is
 457 the volume fraction of molecule i . Such an activity coefficient model was used
 458 in conjunction with equation (1) after setting parameter s to 2 and parameter
 459 Λ to -0.52398 (this is the value proposed by Michelsen during the derivation
 460 of the modified Huron-Vidal mixing rule [77]). As was done previously with
 461 the PPR78 EoS model, the objective function defined by equation (11) was
 462 minimized. The optimal parameters, determined for each isothermal group of
 463 data, are reported in Table 9. Both A_{NO-SO_2} and A_{SO_2-NO} vary according
 464 to the temperature, and the application of a curve fitting leads to polynomial
 465 functions of degree two allowing temperature interpolations.

466 Figure 3 shows data points and results of calculations obtained after coupling
 467 the PR EoS with the two-parameter $a_{res}^{\gamma Wilson}$ model (dashed lines). Such a figure
 468 clearly demonstrates that the correlation of both the critical regions and the dew
 469 curves have been highly improved as compared to PR with one-parameter a^E
 470 model (solid lines).

Table 9: Parameters A_{12} and A_{21} of the Wilson a^E model to use with the advanced mixing rules employed in this study.

$T(\text{K})$	273.15	293.15	313.15	324.15	345.15
A_{NO-SO_2}	180	238	423	603	830
A_{SO_2-NO}	180	-57	-299	-420	-533

471 *3.3. Henry constants of gases in water*

472 The Henry constant (K_H) provides information about interactions between
 473 the solute and the solvent. At T and P conditions, the Henry constant for a
 474 solute i (*i.e.* gas, in this work) in a solvent (*i.e.* water or brines, in this work)
 475 is defined as follows:

$$K_H(T,P) = \lim_{x_i \rightarrow 0} \frac{f_i}{x_i}, \quad (13)$$

476 where f_i and x_i are the fugacity and the mole fraction of the solute i , respec-
 477 tively. f_i is related to the excess chemical potential ($\bar{\mu}_i(T,P,x_i)$) by:

$$\frac{f_i}{x_i} = P \exp(\beta \bar{\mu}_i(T,P,x_i)), \quad (14)$$

478 where $\beta = 1/k_b T$ and k_b is the Boltzmann's constant. Solubilities of gases
 479 in a solvent have been computed using the Widom test insertion technique
 480 which consists in randomly inserting a particle in the solvent. The difference
 481 in potential energy (ΔU^+) resulting from the particle insertion in the solvent
 482 is calculated, and the excess chemical potential at infinite dilution is evaluated
 483 using equation (15).

$$\bar{\mu}_i(T,P,x_i) = -\frac{1}{\beta} \ln \left\langle \frac{\beta P V}{N+1} \exp(-\beta \Delta U^+) \right\rangle_{NpT}, \quad (15)$$

484 with V the volume of the system, see reference [78] for more details.

485 We performed MC simulations in the NpT ensemble for SO_2/H_2O , NO/H_2O
 486 systems, and for three other systems: CO_2/H_2O , O_2/H_2O , and N_2/H_2O , in or-
 487 der to obtain Henry constant values. Temperatures ranged from 273.15 K to

488 623.15 K, and the pressure was set to the corresponding vapour pressure, P^{sat} ,
489 of water. Simulation boxes contained 10^3 water molecules represented with the
490 TIP4P/2005 potential, as this latter is known to better reproduce liquid den-
491 sities as compared to the SPC/E potential [52, 53]. Note that no finite size
492 effect has been detected by Orozco *et al.* using simulation boxes with 300 water
493 molecules [79]. Gas molecules were described using force fields listed in Table 2.
494 For each system, 5×10^8 MC configurations were generated and K_H evaluated us-
495 ing equations (14) and (15). The statistical uncertainty associated to simulated
496 K_H value is 20%, determined using the block averaging technique [74]. Lísal
497 *et al.* have generated K_H values for CO₂ using MC simulations together with
498 SPC based water potentials and three potentials including the EPM2 to mimic
499 CO₂ behavior, and authors showed that the combination SPC/E – EPM2 qual-
500 itatively predicts the temperature dependence of the Henry constant [78]. This
501 latter combination fails in reproducing the maximum in K_H experimentally ob-
502 served at *ca.* 420 K which corresponds to the temperature at which the enthalpy
503 of solution is zero [78, 80]. More recently, Orozco *et al.* showed that K_H values
504 obtained with TIP4P/2005 – EPM2 are lower than predictions using SPC/E
505 – EPM2 [79]. Simultaion results reported in Table 10 supplement these latter
506 data with K_H values for temperatures up to 623.15 K, using the TIP4P/2005
507 – EPM2 model. The simulated maximum in K_H is observed at *ca.* 450 K, but
508 simulation results overestimate experimental K_H values. Molecular simulations
509 were also performed to obtain K_H values for SO₂, NO, O₂, and N₂ in water
510 for temperatures ranging from 273.15 K to 623.15 K, see Table 10. Figure 6
511 illustrates K_H evolutions as a function of the temperature, for gases of interest.
512 Beside NO, molecular simulation results reasonably agree with correlations of
513 experimental values [81, 82], and the temperature value at which the enthalpy
514 of solution is zero – the maximum in K_H – is well estimated.

515 3.4. Solubility of sulphur dioxide in pure water

516 In the case of sulphur dioxide (gas with the lowest K_H values in Table 10),
517 we propose to supplement the information (Henry constant values) provided in

Table 10: Simulated Henry constants for SO₂, CO₂, NO, O₂, and N₂ in water for temperatures ranging from 273.15 K to 623.15 K.

Temperature (K)	Henry constant (MPa.mol/mol)				
	SO ₂	CO ₂	NO	O ₂	N ₂
273.15	3	174	1826	2308	6172
323.15	36	510	4838	6333	15683
373.15	70	885	6150	6871	14354
423.15	104	934	5061	5252	9522
473.15	134	976	3447	3806	6167
523.15	150	808	2185	2354	3405
573.15	138	564	1252	1390	1836
623.15	120	360	671	708	854

518 Table 10 by computing SO₂ solubility in water at higher pressure values beyond
519 the Henry regime. At the two investigated temperatures (298.15 K and 323.15
520 K), phase diagrams for the SO₂ + H₂O binary mixtures exhibit a liquid vapour
521 (L1,V) equilibrium domain at the lowest pressures, a liquid-liquid (L1,L2) equi-
522 librium domain at the highest pressures, with a three-phase line (L1,L2,V) in
523 between these two domains, and a tiny liquid vapour (L2,V) domain just above
524 the three-phase line near the pure SO₂ axis. MC molecular simulations were
525 performed in the Gibbs ensemble for pressures up to 10 MPa, in the Gibbs- NpT
526 ensemble for diphasic systems and in the Gibbs-NVT ensemble for triphasic
527 systems. The studied systems contained in between 550 and 1000 molecules.
528 For each MC simulation, the number of generated configurations ranged within
529 $2 \cdot 10^8$ and $4 \cdot 10^8$ including the equilibration of the system and the production run.
530 Table 11 presents simulated phase compositions for the SO₂ + H₂O systems,
531 and Figure 7 proposes comparisons with available experimental data, for the
532 H₂O-rich part of the pressure-composition diagram. Table 11 contains informa-
533 tion regarding coordinates of the three-phase line in between the vapour-liquid
534 and the liquid-liquid equilibrium domains, located at 0.41 MPa and 0.86 MPa
535 at 298.15 K and 323.15 K, respectively. Comparisons with available experimen-

536 tal data performed in Figure 7 indicate that the SO₂ content of the water-rich
537 branch of the liquid-liquid domain is slightly underestimated by molecular sim-
538 ulations. Using solubility data presented in Table 11, one can estimate Henry
539 constant values: 9 MPa.mol/mol at 298.15 K and 33 MPa.mol/mol at 323.15
540 K, in line with values reported in Table 10.

541 3.5. Liquid densities and osmotic pressures for brines

542 For binary H₂O/NaCl and H₂O/CaCl₂ systems, we propose to supplement
543 the information available in the literature regarding the prediction of brine
544 liquid density values using non-polarizable intermolecular potentials. Thus, we
545 performed HMCMD simulations in the NpT ensemble for NaCl or CaCl₂ aque-
546 ous solutions with molalities from 0 to 5 mol.kg⁻¹, at 298 K and 0.1 MPa. Our
547 simulation boxes contain 500 water molecules and up to 45 salt molecules (NaCl
548 or CaCl₂). We did not investigate size effects but Tsai *et al.*, who considered
549 similar binary systems with smaller simulation box size, have reported no or
550 negligible finite-size effects [63].

551 Table 12 details obtained simulated density values for NaCl aqueous solu-
552 tions at 298 K and 0.1 MPa. Figure 8 presents the simulated density values as
553 a function of brine molal concentrations for each of the considered couple water
554 – NaCl models. Predictions obtained with all combinations follow the exper-
555 imental trend, *i.e.* the binary system density increases with the salt molality.
556 Among the tested combinations, TIP4P/2005 – OPLS leads to the most accu-
557 rate predictions with respect to experimental data proposed by Zhang and Han
558 [83], with a MAE of 2.5 kg.m⁻³. The use of the SPC/E – OPLS combinaison
559 leads to a similar predictive accuracy with a MAE of 2.6 kg.m⁻³. Although
560 the Wheeler potential has been designed using the SPC/E model, its combi-
561 nation with the TIP4P/2005 water model results in satisfactory predictions
562 with a MAE of 4.0 kg.m⁻³. The use of other tested combinations significantly
563 underestimates density values for all investigated salt molalities. The osmotic
564 pressure is an interesting thermodynamic property to evaluate the accuracy of
565 force fields for concentrated aqueous salt solutions. MD simulations were per-

Table 11: Phase compositions for the $\text{SO}_2 + \text{H}_2\text{O}$ binary systems at 298.15 K and 323.15 K, obtained using MC molecular simulation. V denotes the vapour phase, and L1 and L2 stand for H_2O -rich and SO_2 -rich liquids, respectively. Water molecules are mimicked using the TIP4P/2005 potential.

P (MPa)	Molar fraction of SO_2		
	L1	L2	V
T = 298.15 K			
0.05	0.00429	—	0.98663
0.10	0.01071	—	0.99304
0.41	0.04427	0.99020	0.99833
0.42	—	1.00000	1.00000
0.50	0.04040	0.98755	—
1.00	0.04124	0.98879	—
3.00	0.04143	0.98819	—
5.00	0.04254	0.99163	—
10.00	0.04229	0.97244	—
T = 323.15 K			
0.05	0.00165	—	0.93193
0.10	0.00397	—	0.96244
0.50	0.01547	—	0.99275
0.86	0.04312	0.98178	0.99588
0.91	—	1.00000	1.00000
1.00	0.03925	0.98104	—
3.00	0.04412	0.97657	—
5.00	0.03935	0.97821	—
10.00	0.03444	0.97999	—

566 formed for the TIP4P/2005 – OPLS and the SPC/E – OPLS combinations,
567 considering four salt molal concentrations (m from 1.0 to 4.5 mol.kg⁻¹), at 298
568 K. Table 14 presents simulation results, and Figure 9(A) proposes a comparison
569 of predicted values with experimental data extracted from reference [84]. The
570 comparison shows that osmotic pressure values obtained with the TIP4P/2005
571 – OPLS combination are in better agreement with respect to reference exper-
572 imental data (MAE = 0.4 MPa) as compared to osmotic pressures calculated
573 with the SPC/E – OPLS combination (MAE = 1.5 MPa). Consequently, the
574 TIP4P/2005 – OPLS will be the only combination considered hereafter for
575 binary H₂O/NaCl systems.

576 Table 13 summarizes density values for aqueous CaCl₂ solutions, using HM-
577 CMD simulations at 298 K and 0.1 MPa. Figure 8 presents the simulated density
578 values as a function of brine molal concentrations for each of the considered cou-
579 ple water – CaCl₂ models. Results show that the best density predictions are
580 obtained using the potential developed by Goo *et al.* and the TIP4P/2005 water
581 models, with a MAE of 7.6 kg.m⁻³. Tsai *et al.* recently studied CaCl₂ aqueous
582 solutions by means of molecular simulations and only SPC based water models,
583 and concluded that the SPC/E – Aqv outperforms all other tested combina-
584 tions. From comparisons performed in Figure 8, we demonstrate that when
585 using SPC/E water model, more accurate density predictions can be obtained
586 with the potential developed by Goo *et al.*, with a MAE of 9.6 kg.m⁻³. Then,
587 MD simulations were performed using the TIP4P/2005 – GoT and the SPC/E
588 – GoS combinations, and simulation conditions similar to those performed in
589 the case of NaCl aqueous solutions in order to investigate osmotic pressures.
590 Table 14 presents simulation results, and Figure 9(B) proposes a comparison
591 of predicted values with experimental data extracted from the work of Staples
592 and Nuttall [85]. Comparisons show that none of the two investigated combina-
593 tions successfully reproduces experimental osmotic pressure values, with MAE
594 greater than 20 MPa. Hereafter, the TIP4P/2005 – GoT model will be used to
595 mimic the behavior of CaCl₂ aqueous solutions.

Table 12: Simulated liquid density values for aqueous NaCl solutions varying the salt molal concentration from 0 to 5 mol.kg⁻¹, at 298 K and 0.1 MPa, obtained using HMCMD simulations in the NpT ensemble and force fields listed in Table 3.

Water – NaCl models	m (mol.kg ⁻¹)	Density (kg.m ⁻³)	Water – NaCl models	m (mol.kg ⁻¹)	Density (kg.m ⁻³)
TIP4P/2005	0	997.6	TIP4P/2005 – Whee	1	1038.2
TIP4P/2005 – OPLS	1	1038.9		2	1071.9
	2	1074.8		3	1102.3
	3	1110.1		4	1129.8
	4	1140.3		5	1157.2
	5	1164.5	SPC/E	0	999.0
TIP4P/2005 – GoT	1	1036.4	SPC/E – OPLS	1	1035.6
	2	1069.7		2	1071.5
	3	1098.4		3	1106.6
	4	1126.4		4	1132.9
	5	1148.0		5	1159.1
TIP4P/2005 – Aqv	1	1030.1	SPC/E – GoS	1	1032.7
	2	1060.7		2	1060.5
	3	1082.1		3	1088.6
	4	1105.6		4	1116.8
	5	1123.9		5	1136.2

Table 13: Simulated liquid density values for aqueous CaCl_2 solutions varying the salt molal concentration from 0 to 5 mol.kg^{-1} , at 298 K and 0.1 MPa, obtained using HMCMD simulations in the NpT ensemble and force fields listed in Table 4.

Water – CaCl_2 models	m (mol.kg^{-1})	Density (kg.m^{-3})	Water – CaCl_2 models	m (mol.kg^{-1})	Density (kg.m^{-3})
TIP4P/2005	0	997.6	SPC/E	0	999.0
TIP4P/2005 – Aqv	1	1078.0	SPC/E – GoS	1	1083.3
	2	1143.7		2	1152.6
	3	1196.1		3	1217.9
	4	1232.4		4	1273.4
	5	1264.3		5	1315.6
TIP4P/2005 – Matt	1	1061.3	SPC/E – Pred	1	1077.2
	2	1108.1		2	1135.2
	3	1156.9		3	1186.8
	4	1194.2		4	1218.4
	5	1231.2		5	1252.7
TIP4P/2005 – GoT	1	1082.4	SPC/E – Aqv	1	1077.1
	2	1152.6		2	1137.9
	3	1218.7		3	1193.2
	4	1273.5		4	1225.7
	5	1326.5		5	1266.6

Table 14: Osmotic pressure values (MPa) for aqueous NaCl and CaCl_2 solutions varying the salt molal concentration from 1 to 5 mol.kg^{-1} , at 298 K and 0.1 MPa, obtained using MD simulations in the NVT ensemble and force fields listed in Tables 3 and 4.

m	NaCl		CaCl ₂				
	TIP4P/2005 – OPLS	m	SPC/E – OPLS	m	TIP4P/2005 – GoT	m	SPC/E – GoS
1.04	4.22	1.03	4.82	1.0	4.82	1.0	6.98
2.19	10.27	2.10	9.34	2.3	13.56	2.3	17.00
3.51	18.73	3.33	19.04	3.6	22.67	3.6	30.59
4.49	24.36	4.48	27.78	4.9	38.51	4.9	49.07

596 *3.6. Henry constants of gases in brines*

597 We performed MC simulations in the NpT ensemble to compute Henry con-
 598 stant values for SO_2 , CO_2 , NO , O_2 , and N_2 in brines. Investigated temperatures
 599 ranged from 298.15 K to 373.15 K, and the pressure was set to the correspond-
 600 ing vapour pressure of the brine which is assumed similar to that of water in
 601 the range of investigated salt concentrations. From conclusions drawn in previ-
 602 ous sections, simulation boxes contained 10^3 water molecules represented with
 603 the TIP4P/2005 potential, and NaCl and CaCl_2 mimicked using the OPLS (see
 604 Table 3) and GoT (see Table 4) parameterizations, respectively. Gas molecules
 605 were described using force fields listed in Table 2. Up to 2×10^9 MC configura-
 606 tions were generated for each system, and K_H evaluated according to equations
 607 (13) to (15). The mole fraction of the solute (gas molecule inserted in the sim-
 608 ulation box) is defined as $1/(N+1)$, with N the number of solvent species in the
 609 simulation box. In the case of brines, N can be estimated either considering
 610 anions and cations coupled or not; salt ions are supposed uncoupled hereafter.
 611 Due to the low acceptance of insertions for high salt concentrations and result-
 612 ing problems of statistics, we chose to limit the present study to brines with salt
 613 molalities up to 3 mol.kg^{-1} . Tables 15 and 16 report simulated Henry constant
 614 values for NaCl and CaCl_2 aqueous solutions, respectively. Figure 10 illustrates
 615 K_H values simulated for gases in NaCl aqueous solutions. The statistical un-
 616 certainty associated to simulated K_H value is 20%, determined using the block
 617 averaging technique [74]. Our proposed sets of simulated Henry constant values
 618 can be used to estimate Sechenov constant (K_S) values as defined in equation
 619 (16) [86, 87].

$$\log \left(\frac{K_H^b}{K_H^w} \right) = K_S \cdot m, \quad (16)$$

620 where m is the salt molality, and K_H^w and K_H^b denotes Henry constants in water
 621 and brine, respectively. For studied temperatures and NaCl brines, K_S values
 622 for CO_2 , NO , O_2 , and N_2 in NaCl aqueous solutions lie in between 0.11 and
 623 0.15 kg.mol^{-1} , and K_S values for SO_2 range from 0.07 to 0.22 kg.mol^{-1} . In the

Table 15: Simulated Henry constants for some gases in NaCl aqueous solutions for temperatures ranging from 298.15 K to 373.15 K.

Temperature (K)	m (mol.kg ⁻¹)	Henry constant (MPa.mol/mol)				
		SO ₂	CO ₂	NO	O ₂	N ₂
298.15	1	20	548	6225	7288	18861
	2	39	744	10273	11813	33861
	3	55	909	12209	14389	38511
323.15	1	48	845	8222	9362	23340
	2	64	1318	11935	13672	36873
	3	84	1295	13945	15868	41267
373.15	1	87	1298	8683	9675	21086
	2	102	1734	11747	13177	29267
	3	111	2248	15739	17627	39944

624 case of CaCl₂ aqueous solutions, simulated K_S values range from 0.07 to 0.20
625 kg.mol⁻¹. Considering uncertainties on simulated K_H values, simulated K_S are
626 in agreement with estimations obtained using the Schumpe and Weisenberger
627 model with predicted K_S in between -0.02 and 0.28 kg.mol⁻¹ for the same
628 systems [88, 89].

629 3.7. Solubility of sulphur dioxide in brines

630 We propose to supplement information contained in Tables 15 and 16 com-
631 puting SO₂ solubility in NaCl and CaCl₂ aqueous solutions at higher pressure
632 values. For the two investigated temperatures (298.15 K and 323.15 K), phase
633 diagrams for the SO₂ + brine mixtures exhibit a VL equilibrium domain at the
634 lowest pressures and a liquid-liquid equilibrium domain at the highest pressures,
635 with a three-phase line in between these two domains. MC molecular simula-
636 tions were performed in the Gibbs ensemble for pressures up to 10 MPa, in the
637 Gibbs- NpT ensemble for diphasic systems and in the Gibbs-NVT ensemble for
638 triphasic systems. Note that an additional constraint prevents the transfer of
639 ions from the liquid to the vapour phase. For each MC simulation, the number
640 of generated configurations ranged within 7.10^8 and 8.10^8 including the equi-

Table 16: Simulated Henry constants for some gases in CaCl₂ aqueous solutions for temperatures ranging from 323.15 K to 373.15 K.

Temperature (K)	m (mol.kg ⁻¹)	Henry constant (MPa.mol/mol)				
		SO ₂	CO ₂	NO	O ₂	N ₂
298.15	1	43	643	8155	9208	27339
	2	67	942	10880	12387	36286
	3	72	1587	18655	21145	63282
323.15	1	47	825	8723	9861	25073
	2	53	1237	12593	14174	37067
	3	60	1862	15225	17495	45923
373.15	1	123	1533	9722	10816	24196
	2	189	2441	14181	15793	36816
	3	253	3115	18332	20281	46899

641 liberation of the system and the production run. Table 17 presents simulated
642 phase compositions for SO₂ + brines (H₂O/NaCl and H₂O/CaCl₂, 3 mol.kg⁻¹)
643 systems for temperatures in between 298.15 K and 373.15 K. Table 17 contains
644 information regarding coordinates of the three-phase line in between the vapour-
645 liquid and the liquid-liquid equilibrium domains in the case of NaCl brines. For
646 these systems, obtained three-phase line pressures are similar to pure water
647 cases with 0.40 MPa and 0.89 MPa at 298.15 K and 323.15 K, respectively.
648 Note that no attempt to capture the three-phase line has been done in the case
649 of SO₂ + H₂O/CaCl₂ systems. Using solubility data presented in Table 17,
650 one can estimate Henry constant values of SO₂ in a NaCl (3 mol.kg⁻¹) aqueous
651 solution: 41 MPa.mol/mol at 298.15 K and 72 MPa.mol/mol at 323.15 K, in
652 agreement with values reported in Table 15. Using solubility data presented in
653 Table 17, one can also estimate Henry constant values for SO₂ in a CaCl₂ (3
654 mol.kg⁻¹) aqueous solutions: 51 MPa.mol/mol at 298.15 K, 59 MPa.mol/mol at
655 323.15 K and 257 MPa.mol/mol at 373.15 K, in agreement with values reported
656 in Table 16.

Table 17: Phase compositions for the SO₂ + brine (H₂O/NaCl and H₂O/CaCl₂, with a salt molal concentration of 3 mol.kg⁻¹) systems at different temperatures, obtained using MC molecular simulation. V denotes the vapour phase, and L1 and L2 stand for H₂O-rich and SO₂-rich liquids, respectively.

P (MPa)	Molar fraction of SO ₂			P (MPa)	Molar fraction of SO ₂		
	L1	L2	V		L1	L2	V
	H ₂ O + NaCl, 298.15 K				H ₂ O + CaCl ₂ , 298.15 K		
0.05	0.0012	—	0.9862	0.05	0.0022	—	0.9877
0.10	0.0035	—	0.9935	0.10	0.0036	—	0.9945
0.50	0.0124	—	0.9986	0.50	0.0112	—	0.9986
0.40	0.0107	0.9912	0.9984	1.00	0.0321	0.9916	—
1.00	0.0198	0.9926	—		H ₂ O + CaCl ₂ , 323.15 K		
3.00	0.0202	0.9923	—	0.05	0.0004	—	0.9434
5.00	0.0382	0.9878	—	0.10	0.0014	—	0.9725
10.00	0.0120	0.9929	—	0.50	0.0081	—	0.9937
	H ₂ O + NaCl, 323.15 K			1.00	0.0268	0.9858	—
0.05	0.0008	—	0.9407		H ₂ O + CaCl ₂ , 373.15 K		
0.10	0.0013	—	0.9699	0.05	0.0001	—	0.3737
0.50	0.0074	—	0.9932	0.10	0.0003	—	0.6724
0.89	0.0123	0.9844	0.9960	0.50	0.0018	—	0.9321
1.00	0.0135	0.9846	—	1.00	0.0157	0.9604	—
3.00	0.0132	0.9856	—				
5.00	0.0133	0.9849	—				
10.00	0.0101	0.9843	—				

657 4. Conclusions

658 In the present work, we have proposed new insights for NO + SO₂ bi-
659 nary systems, using molecular simulation techniques, equations of state, and
660 experiments. Using intermolecular potentials available in the literature we have
661 demonstrated the capability of molecular simulation techniques in predicting
662 properties for mixtures. Solubilities of some gases (CO₂ and associated gases
663 such as O₂, N₂, SO₂, NO) in water and in NaCl and CaCl₂ aqueous solutions
664 have also been studied using molecular simulation techniques. In the case of
665 the highest soluble gases (*e.g.*, sulphur dioxide) reasonable simulation box size
666 can be envisaged and explicit analysis of phase compositions performed. For
667 gas with low solubility value (CO₂, O₂, N₂, and NO) we only determined Henry
668 constants.

669 Results of performed quantum chemical calculations tend to indicate no
670 favoured chemical reaction between NO and SO₂ in the gas phase. In addition,
671 no evidence of such chemical reaction has been observed during the experimen-
672 tal data acquisition. New sets of experimental vapour compositions have been
673 proposed for NO + SO₂ binary mixtures. Data generated using molecular simu-
674 lations agree fairly well with reference experimental data. Using the so-obtained
675 data, we proposed new sets of parameters for the PPR78 EoS model. Henry
676 constant values for gases in water generated by means of molecular simulations
677 fairly agree with reference data. The performed study on the ability of various
678 potentials in predicting sodium chloride and calcium chloride brine densities
679 and osmotic pressures led us to recommend two sets of parameters, both in-
680 volving the TIP4P/2005 water potential. Finally, Henry constant values for
681 gases in sodium chloride and calcium chloride brines were generated by means
682 of molecular simulations.

683 In this work, we show that combining some experiments, molecular simula-
684 tions and equation of state modelling is relevant to fill the lack of information
685 for gas mixtures representative of systems encountered in CCS operations. Us-
686 ing validated intermolecular potentials, molecular simulations is an interesting

687 tool to generate data, especially when hazardous compounds and/or extreme
688 pressure or temperature conditions are considered. Simulated data can then
689 be used to optimize equations of state parameters, and thus to improve models
690 implemented within geochemical codes.

691 **Acknowledgement**

692 The financial support from the French Agence Nationale de la Recherche,
693 ANR, for the SIGARRR project (ANR-13-SEED-006) is gratefully acknowl-
694 edged. Authors would like to thank Dr Bernard Rousseau for the use of the
695 NEWTON Molecular Dynamics code.

696 **References**

- 697 [1] United Nation Framework Convention on Climate Change, Adoption of the
698 Paris Agreement, Technical Report, 2015.
- 699 [2] A. Torvanger, M. T. Lund, N. Rive, Carbon capture and storage deploy-
700 ment rates: needs and feasibility, *Mitigation and Adaptation Strategies for*
701 *Global Change* 18 (2013) 187–205.
- 702 [3] S. Thibeau, P. Chiquet, G. Mouronval, M. Lescanne, Geochemical assess-
703 ment of the injection of CO₂ into rousse depleted gas reservoir, *Energy*
704 *Procedia* 1 (2009) 3383–3390.
- 705 [4] M. Lescanne, J. Hy-Billiot, N. Aimard, C. Prinnet, The site monitoring
706 of the Lacq industrial CCS reference project, *Energy Procedia* 4 (2011)
707 3518–3525.
- 708 [5] B. Garcia, J. Hy-Billiot, V. Rouchon, G. Mouronval, M. Lescanne, V. La-
709 chet, N. Aimard, A geochemical approach for monitoring a CO₂ pilot site:
710 Rousse, france. a major gases, CO₂ - carbon isotopes and noble gases com-
711 bined approach, *Oil & Gas Science and Technology – Revue d’IFP Energies*
712 *nouvelles* 67 (2012) 341–353.
- 713 [6] B. Creton, T. d. Bruin, D. Le Roux, P. Duchet-Suchaux, V. Lachet, Im-
714 pact of associated gases on equilibrium and transport properties of a CO₂
715 stream: Molecular simulation and experimental studies, *International Jour-*
716 *nal of Thermophysics* 35 (2014) 256–276.
- 717 [7] J. Sterpenich, J. Dubessy, J. Pironon, S. Renard, M.-C. Caumon, A. Randi,
718 J.-N. Jaubert, E. Favre, D. Roizard, M. Parmentier, M. Azaroual, V. La-
719 chet, B. Creton, T. Parra, E. E. Ahmar, C. Coquelet, V. Lagneau,
720 J. Corvisier, P. Chiquet, Role of impurities on CO₂ injection: Experimental
721 and numerical simulations of thermodynamic properties of water-salt-gas
722 mixtures (CO₂ + co-injected gases) under geological storage conditions,
723 *Energy Procedia* 37 (2013) 3638–3645.

- 724 [8] J. Corvisier, E. E. Ahmar, C. Coquelet, J. Sterpenich, R. Privat, J.-N.
725 Jaubert, K. Ballerat-Busserolles, J.-Y. Coxam, P. Cézac, F. Contamine,
726 J.-P. Serin, V. Lachet, B. Creton, M. Parmentier, P. Blanc, L. André, L. d.
727 Lary, E. C. Gaucher, Simulations of the impact of co-injected gases on
728 CO₂ storage, the SIGARRR project: First results on water-gas interactions
729 modeling, *Energy Procedia* 63 (2014) 3160–3171.
- 730 [9] J. Corvisier, M. Hajiw, E. El Ahmar, C. Coquelet, J. Sterpenich, R. Privat,
731 J.-N. Jaubert, K. Ballerat-Busserolles, J.-Y. Coxam, P. Cézac, F. Con-
732 tamine, J.-P. Serin, V. Lachet, B. Creton, M. Parmentier, J. Tremosa,
733 P. Blanc, L. André, L. de Lary, E. Gaucher, Simulations of the impact of
734 co-injected gases on CO₂ storage, the SIGARRR project: Processes and
735 geochemical approaches for gas-water-salt interactions modeling, *Energy*
736 *Procedia* 114 (2017) 3322–3334. 13th International Conference on Green-
737 house Gas Control Technologies, GHGT-13, 14-18 November 2016, Lau-
738 sanne, Switzerland.
- 739 [10] A. Estublier, P. Bachaud, A. Michel, N. Maurand, J.-P. Deflandre, Long-
740 term fate of CO₂ in a saline aquifer: modeling issues, *Energy Procedia* 63
741 (2014) 3464–3474.
- 742 [11] C. Haase, A. Dahmke, M. Ebert, D. Schäfer, F. Dethlefsen, Suitability
743 of existing numerical model codes and thermodynamic databases for the
744 prognosis of calcite dissolution processes in near-surface sediments due to
745 a CO₂ leakage investigated by column experiments, *Aquatic Geochemistry*
746 20 (2014) 639–661.
- 747 [12] C. Haase, M. Ebert, F. Dethlefsen, Uncertainties of geochemical codes and
748 thermodynamic databases for predicting the impact of carbon dioxide on
749 geologic formations, *Applied Geochemistry* 67 (2016) 81–92.
- 750 [13] D.-Y. Peng, D. B. Robinson, A new two-constant equation of state, *Indus-*
751 *trial & Engineering Chemistry Fundamentals* 15 (1976) 59–64.

- 752 [14] H. Li, J. P. Jakobsen, Ø. Wilhelmsen, J. Yan, Pvtxy properties of CO₂
753 mixtures relevant for CO₂ capture, transport and storage: Review of avail-
754 able experimental data and theoretical models, *Applied Energy* 88 (2011)
755 3567–3579.
- 756 [15] H. Li, Ø. Wilhelmsen, Y. Lv, W. Wang, J. Yan, Viscosities, thermal con-
757 ductivities and diffusion coefficients of CO₂ mixtures: Review of experi-
758 mental data and theoretical models, *International Journal of Greenhouse*
759 *Gas Control* 5 (2011) 1119–1139.
- 760 [16] X. Xu, R. Privat, J.-N. Jaubert, Addition of the sulfur dioxide group (SO₂),
761 the oxygen group (O₂), and the nitric oxide group (NO) to the E-PPR78
762 model, *Industrial & Engineering Chemistry Research* 54 (2015) 9494–9504.
- 763 [17] X. Xu, R. Privat, J.-N. Jaubert, V. Lachet, B. Creton, Phase equilibrium
764 of CCS mixtures: Equation of state modeling and monte carlo simulation,
765 *The Journal of Supercritical Fluids* 119 (2017) 169–202.
- 766 [18] E. Bourasseau, V. Lachet, N. Desbiens, J.-B. Maillet, J.-M. Teuler, P. Un-
767 gerer, Thermodynamic behavior of the CO₂ + NO₂/N₂O₄ mixture: a
768 monte carlo simulation study, *The Journal of Physical Chemistry B* 112
769 (2008) 15783–15792.
- 770 [19] V. Lachet, T. de Bruin, P. Ungerer, C. Coquelet, A. Valtz, V. Hasanov,
771 F. Lockwood, D. Richon, Thermodynamic behavior of the CO₂+SO₂ mix-
772 ture: Experimental and monte carlo simulation studies, *Energy Procedia*
773 1 (2009) 1641–1647.
- 774 [20] E. El Ahmar, B. Creton, A. Valtz, C. Coquelet, V. Lachet, D. Richon,
775 P. Ungerer, Thermodynamic study of binary systems containing sulphur
776 dioxide: Measurements and molecular modelling, *Fluid Phase Equilibria*
777 304 (2011) 21–34.
- 778 [21] V. Lachet, B. Creton, T. de Bruin, E. Bourasseau, N. Desbiens, Ø. Wil-
779 helmsen, M. Hammer, Equilibrium and transport properties of CO₂+N₂O

- 780 and CO₂+NO mixtures: Molecular simulation and equation of state mod-
781 elling study, *Fluid Phase Equilibria* 322-323 (2012) 66–78.
- 782 [22] C. Coquelet, A. Valtz, P. Arpentinier, Thermodynamic study of binary
783 and ternary systems containing CO₂ + impurities in the context of CO₂
784 transportation, *Fluid Phase Equilibria* 382 (2014) 205–211.
- 785 [23] ARMINES, Patent no fr 2 853 414, procédé et dispositif pour prélever
786 des micro échantillons d’un fluide sous pression contenu dans un container,
787 2003.
- 788 [24] S. Lasala, P. Chiesa, R. Privat, J.-N. Jaubert, VLE properties of CO₂-based
789 binary systems containing N₂, O₂ and Ar: Experimental measurements
790 and modelling results with advanced cubic equations of state, *Fluid Phase*
791 *Equilibria* 428 (2016) 18–31.
- 792 [25] S. Lasala, P. Chiesa, R. Privat, J.-N. Jaubert, Measurement and pre-
793 diction of multi-property data of CO₂-N₂-O₂-CH₄ mixtures with the Peng-
794 Robinson +residual Helmholtz energy-based model, *Fluid Phase Equilibria*
795 437 (2017) 166–180.
- 796 [26] S. Lasala, P. Chiesa, R. Privat, J.-N. Jaubert, Modeling the thermody-
797 namics of fluids treated by CO₂ capture processes with Peng-Robinson
798 +residual Helmholtz energy-based mixing rules, *Industrial & Engineering*
799 *Chemistry Research* 56 (2017) 2259–2276.
- 800 [27] Y. Le Guennec, S. Lasala, R. Privat, J.-N. Jaubert, A consistency test for
801 α -functions of cubic equations of state, *Fluid Phase Equilibria* 427 (2016)
802 513–538.
- 803 [28] Y. Le Guennec, R. Privat, J.-N. Jaubert, Development of the translated-
804 consistent tc-pr and tc-rk cubic equations of state for a safe and accurate
805 prediction of volumetric, energetic and saturation properties of pure com-
806 pounds in the sub- and super-critical domains, *Fluid Phase Equilibria* 429
807 (2016) 301–312.

- 808 [29] Y. Le Guennec, R. Privat, S. Lasala, J.-N. Jaubert, On the imperative need
809 to use a consistent α -function for the prediction of pure-compound super-
810 critical properties with a cubic equation of state, *Fluid Phase Equilibria*
811 445 (2017) 45–53.
- 812 [30] J.-N. Jaubert, R. Privat, Y. Le Guennec, L. Coniglio, Note on the prop-
813 erties altered by application of a péneloux-type volume translation to an
814 equation of state, *Fluid Phase Equilibria* 419 (2016) 88–95.
- 815 [31] R. Privat, J.-N. Jaubert, Y. Le Guennec, Incorporation of a volume trans-
816 lation in an equation of state for fluid mixtures: which combining rule?
817 which effect on properties of mixing?, *Fluid Phase Equilibria* 427 (2016)
818 414–420.
- 819 [32] X. Xu, S. Lasala, R. Privat, J.-N. Jaubert, E-PPR78: A proper cubic EoS
820 for modelling fluids involved in the design and operation of carbon dioxide
821 capture and storage (CCS) processes, *International Journal of Greenhouse*
822 *Gas Control* 56 (2017) 126–154.
- 823 [33] J.-N. Jaubert, F. Mutelet, VLE predictions with the Peng-Robinson equa-
824 tion of state and temperature dependent k_{ij} calculated through a group
825 contribution method, *Fluid Phase Equilibria* 224 (2004) 285–304.
- 826 [34] J.-W. Qian, R. Privat, J.-N. Jaubert, Predicting the phase equilibria, criti-
827 cal phenomena, and mixing enthalpies of binary aqueous systems containing
828 alkanes, cycloalkanes, aromatics, alkenes, and gases (N_2 , CO_2 , H_2S , H_2)
829 with the PPR78 equation of state, *Industrial & Engineering Chemistry*
830 *Research* 52 (2013) 16457–16490.
- 831 [35] P. Ungerer, B. Tavitian, A. Boutin, *Applications of Molecular Simulation*
832 *in the Oil and Gas Industry - Monte-Carlo Methods*, Editions TECHNIP,
833 2005.
- 834 [36] A. Z. Panagiotopoulos, Direct determination of phase coexistence prop-

- 835 erties of fluids by Monte Carlo simulation in a new ensemble, *Molecular*
836 *Physics* 61 (1987) 813–826.
- 837 [37] A. Panagiotopoulos, N. Quirke, M. Stapleton, D. J. Tildesley, Phase equi-
838 libria by simulation in the Gibbs ensemble, *Molecular Physics* 63 (1988)
839 527–545.
- 840 [38] S. Duane, A. Kennedy, B. J. Pendleton, D. Roweth, Hybrid Monte Carlo,
841 *Physics Letters B* 195 (1987) 216–222.
- 842 [39] V. Lachet, J.-M. Teuler, B. Rousseau, Classical force field for hydrofluoro-
843 carbon molecular simulations. application to the study of gas solubility in
844 poly(vinylidene fluoride), *The Journal of Physical Chemistry A* 119 (2015)
845 140–151.
- 846 [40] N.-T. Van-Oanh, C. Houriez, B. Rousseau, Viscosity of the 1-ethyl-
847 3-methylimidazolium bis(trifluoromethylsulfonyl)imide ionic liquid from
848 equilibrium and nonequilibrium molecular dynamics, *Physical Chemistry*
849 *Chemical Physics* 12 (2010) 930–936.
- 850 [41] Y. Luo, B. Roux, Simulation of osmotic pressure in concentrated aqueous
851 salt solutions, *The Journal of Physical Chemistry Letters* 1 (2010) 183–189.
- 852 [42] J. G. Harris, K. H. Yung, Carbon dioxide’s liquid-vapor coexistence curve
853 and critical properties as predicted by a simple molecular model, *The*
854 *Journal of Physical Chemistry* 99 (1995) 12021–12024.
- 855 [43] J. Delhommelle, Etablissement de potentiels d’interactions pour la simula-
856 tion moléculaire. Application à la prédiction des équilibres liquide-vapeur
857 de mélanges binaires alcane-molécule multipolaire, Ph.D. Thesis, Université
858 Paris XI, Orsay, France, 2000.
- 859 [44] J. Vrabec, J. Stoll, H. Hasse, A set of molecular models for symmetric
860 quadrupolar fluids, *The Journal of Physical Chemistry B* 105 (2001) 12126–
861 12133.

- 862 [45] Y. Boutard, P. Ungerer, J. M. Teuler, M. G. Ahunbay, S. F. Sabater,
863 J. Pérez-Pellitero, A. D. Mackie, E. Bourasseau, Extension of the
864 anisotropic united atoms intermolecular potential to amines, amides and
865 alkanols, *Fluid Phase Equilibria* 236 (2005) 25–41.
- 866 [46] H. J. C. Berendsen, J. R. Grigera, T. P. Straatsma, The missing term
867 in effective pair potentials, *The Journal of Physical Chemistry* 91 (1987)
868 6269–6271.
- 869 [47] J. L. F. Abascal, C. Vega, A general purpose model for the condensed
870 phases of water: TIP4P/2005, *The Journal of Chemical Physics* 123 (2005)
871 234505.
- 872 [48] C. Nieto-Draghi, T. de Bruin, J. Pérez-Pellitero, J. Bonet Avalos, A. D.
873 Mackie, Thermodynamic and transport properties of carbon dioxide from
874 molecular simulation, *The Journal of Chemical Physics* 126 (2007) 064509.
- 875 [49] B. Guillot, A reappraisal of what we have learnt during three decades of
876 computer simulations on water, *Journal of Molecular Liquids* 101 (2002)
877 219–260.
- 878 [50] L. Vlcek, A. A. Chialvo, D. R. Cole, Optimized unlike-pair interactions for
879 water-carbon dioxide mixtures described by the SPC/E and EPM2 models,
880 *The Journal of Physical Chemistry B* 115 (2011) 8775–8784.
- 881 [51] C. Vega, J. L. F. Abascal, Simulating water with rigid non-polarizable
882 models: a general perspective, *Physical Chemistry Chemical Physics* 13
883 (2011) 19663–19688.
- 884 [52] R. Sakamaki, A. K. Sum, T. Narumi, K. Yasuoka, Molecular dynamics sim-
885 ulations of vapor/liquid coexistence using the nonpolarizable water models,
886 *The Journal of Chemical Physics* 134 (2011) 124708.
- 887 [53] V. Vinš, D. Celný, B. Planková, T. Němec, M. Duška, J. Hrubý,
888 P. Dančová, M. Veselý, Molecular simulations of the vapor-liquid phase

- 889 interfaces of pure water modeled with the SPC/E and the TIP4P/2005
890 molecular models, EPJ Web of Conferences 114 (2016) 02136.
- 891 [54] J. Chandrasekhar, D. C. Spellmeyer, W. L. Jorgensen, Energy compo-
892 nent analysis for dilute aqueous solutions of lithium(1+), sodium(1+),
893 fluoride(1-), and chloride(1-) ions, Journal of the American Chemical So-
894 ciety 106 (1984) 903–910.
- 895 [55] W. L. Jorgensen, D. S. Maxwell, J. Tirado-Rives, Development and testing
896 of the OPLS all-atom force field on conformational energetics and properties
897 of organic liquids, Journal of the American Chemical Society 118 (1996)
898 11225–11236.
- 899 [56] D. R. Wheeler, J. Newman, Molecular dynamics simulations of multicom-
900 ponent diffusion. 1. equilibrium method, The Journal of Physical Chemistry
901 B 108 (2004) 18353–18361.
- 902 [57] G. H. Goo, G. Sung, S. H. Lee, Molecular dynamics simulation studies of
903 the limiting conductances of MgCl_2 and CaCl_2 in supercritical water using
904 SPC/E model for water, Molecular Simulation 30 (2004) 37–44.
- 905 [58] J. Åqvist, Ion-water interaction potentials derived from free energy per-
906 turbation simulations, The Journal of Physical Chemistry 94 (1990) 8021–
907 8024.
- 908 [59] M. M. Reif, P. H. Hünenberger, Computation of methodology-independent
909 single-ion solvation properties from molecular simulations. IV. optimized
910 lennard-jones interaction parameter sets for the alkali and halide ions in
911 water, The Journal of Chemical Physics 134 (2011) 144104.
- 912 [60] J.-C. Neyt, A. Wender, V. Lachet, A. Ghoufi, P. Malfreyt, Prediction
913 of the concentration dependence of the surface tension and density of salt
914 solutions: atomistic simulations using drude oscillator polarizable and non-
915 polarizable models, Physical Chemistry Chemical Physics 15 (2013) 11679–
916 11690.

- 917 [61] J.-C. Neyt, A. Wender, V. Lachet, A. Szymczyk, A. Ghoufi, P. Malfreyt,
918 How does the electronic continuum model perform in the prediction of the
919 surface tension of salt solutions?, *Chemical Physics Letters* 595-596 (2014)
920 209–213.
- 921 [62] G. A. Orozco, O. A. Moulton, H. Jiang, I. G. Economou, A. Z. Pana-
922 giotopoulos, Molecular simulation of thermodynamic and transport prop-
923 erties for the H₂O+NaCl system, *The Journal of Chemical Physics* 141
924 (2014) 234507.
- 925 [63] E. S. Tsai, H. Jiang, A. Z. Panagiotopoulos, Monte carlo simulations of
926 H₂O–CaCl₂ and H₂O–CaCl₂–CO₂ mixtures, *Fluid Phase Equilibria* 407
927 (2016) 262–268.
- 928 [64] R. P. Matthews, K. J. Naidoo, Experimentally consistent ion association
929 predicted for metal solutions from free energy simulations, *The Journal of*
930 *Physical Chemistry B* 114 (2010) 7286–7293.
- 931 [65] L. X. Dang, D. E. Smith, Comment on “mean force potential for the
932 calcium–chloride ion pair in water” [*J. chem. phys.* 99, 4229 (1993)], *The*
933 *Journal of Chemical Physics* 102 (1995) 3483.
- 934 [66] L. X. Dang, Mechanism and thermodynamics of ion selectivity in aqueous
935 solutions of 18-crown-6 ether: A molecular dynamics study, *Journal of the*
936 *American Chemical Society* 117 (1995) 6954–6960.
- 937 [67] M. Předota, Z. Zhang, P. Fenter, D. J. Wesolowski, P. T. Cummings, Elec-
938 tric double layer at the rutile (110) surface. 2. adsorption of ions from molec-
939 ular dynamics and X-ray experiments, *The Journal of Physical Chemistry*
940 *B* 108 (2004) 12061–12072.
- 941 [68] M. J. Frisch, G. W. Trucks, H. B. Schlegel, G. E. Scuseria, M. A.
942 Robb, Cheeseman, G. Scalmani, V. Barone, B. Mennucci, G. A. Peters-
943 son, H. Nakatsuji, M. Caricato, X. Li, H. P. Hratchian, Izmaylov, A. F.,

- 944 J. Bloino, G. Zheng, Sonnenberg, J. L., M. Hada, M. Ehara, K. Toy-
945 ota, R. Fukuda, J. Hasegawa, M. Ishida, T. Nakajima, Y. Honda, O. Ki-
946 tao, H. Nakai, T. Vreven, J. A. Montgomery, Peralta, J. E., F. Ogliaro,
947 M. Bearpark, Heyd, J. J., E. Brothers, K. N. Kudin, Staroverov, V. N.,
948 R. Kobayashi, J. Normand, K. Raghavachari, A. Rendell, J. C. Burant,
949 S. S. Iyengar, J. Tomasi, M. Cossi, N. Rega, J. M. Millam, M. Klene,
950 J. E. Knox, J. B. Cross, V. Bakken, C. Adamo, J. Jaramillo, R. Gomperts,
951 R. E. Stratmann, O. Yazyev, A. J. Austin, R. Cammi, C. Pomelli, J. W.
952 Ochterski, R. L. Martin, K. Morokuma, V. G. Zakrzewski, G. A. Voth,
953 P. Salvador, J. J. Dannenberg, S. Dapprich, A. D. Daniels, Farkas, J. B.
954 Foresman, J. V. Ortiz, J. Cioslowski, D. J. Fox, Gaussian 09, revision b.01,
955 Gaussian 09, Revision B.01, Gaussian, Inc., Wallingford CT (2009).
- 956 [69] Y. Zhao, D. G. Truhlar, The M06 suite of density functionals for main
957 group thermochemistry, thermochemical kinetics, noncovalent interactions,
958 excited states, and transition elements: two new functionals and systematic
959 testing of four M06-class functionals and 12 other function, *Theoretical*
960 *Chemistry Accounts* 120 (2007) 215–241.
- 961 [70] M. Tobita, S. Perera, M. Musial, R. Bartlett, M. Nooijen, J. Lee, Critical
962 comparison of single-reference and multireference coupled-cluster methods:
963 Geometry, harmonic frequencies, and excitation energies of N₂O₂, *The*
964 *Journal of Chemical Physics* 119 (2003) 10713–10723.
- 965 [71] R. Sayós, R. Valero, J. Anglada, M. González, Theoretical investigation of
966 the eight low-lying electronic states of the cis- and trans-nitric oxide dimers
967 and its isomerization using multiconfigurational second-order perturbation
968 theory (CASPT2), *The Journal of Chemical Physics* 112 (2000) 6608–6624.
- 969 [72] A. Dkhissi, P. Soulard, A. Perrin, N. Lacome, The 5NO6 dimer, *Journal*
970 *of Molecular Spectroscopy* 183 (1997) 12–17.
- 971 [73] A. McKellar, J. Watson, B. Howard, The NO dimer: 15 N isotopic infrared
972 spectra, line-widths, and force field, *Molecular Physics* 86 (1995) 273–286.

- 973 [74] M. P. Allen, D. J. Tildesley, Computer simulation of liquids, Oxford Science
974 Publications, Oxford, 1987.
- 975 [75] R. Privat, J.-N. Jaubert, Classification of global fluid-phase equilibrium
976 behaviors in binary systems, Chemical Engineering Research and Design
977 91 (2013) 1807–1839.
- 978 [76] P. Van Konynenburg, R. Scott, Critical lines and phase equilibria in binary
979 van der waals mixtures, Philosophical Transactions of the Royal Society:
980 Mathematical, Physical and Engineering Sciences 298 (1980) 495–540.
- 981 [77] M. Michelsen, A modified Huron-Vidal mixing rule for cubic equations of
982 state, Fluid Phase Equilibria 60 (1990) 213–219.
- 983 [78] M. Lísal, W. R. Smith, K. Aim, Analysis of Henry’s constant for carbon
984 dioxide in water via Monte Carlo simulation, Fluid Phase Equilibria 226
985 (2004) 161–172.
- 986 [79] G. A. Orozco, V. Lachet, A. D. Mackie, Physical absorption of green
987 house gases in amines: The influence of functionality, structure, and cross-
988 interactions, The Journal of Physical Chemistry B 120 (2016) 13136–13143.
- 989 [80] J. J. Carroll, J. D. Slupsky, A. E. Mather, The solubility of carbon dioxide
990 in water at low pressure, Journal of Physical and Chemical Reference Data
991 20 (1991) 1201–1209.
- 992 [81] A. Harvey, Semiempirical correlation for henry’s constants over large tem-
993 perature ranges, AIChE Journal 42 (1996) 1491–1494.
- 994 [82] C. L. Yaws, Chemical properties handbook: physical, thermodynamic, en-
995 vironmental transport, safety, and health related properties for organic and
996 inorganic chemicals, McGraw-Hill, New York, USA, 1999.
- 997 [83] H.-L. Zhang, S.-J. Han, Viscosity and density of water + sodium chlo-
998 ride + potassium chloride solutions at 298.15 K, Journal of Chemical &
999 Engineering Data 41 (1996) 516–520.

- 1000 [84] G. Wilczek-Vera, J. H. Vera, How much do we know about the activity
1001 of individual ions?, *The Journal of Chemical Thermodynamics* 99 (2016)
1002 65–69.
- 1003 [85] B. Staples, R. Nuttall, The activity and osmotic coefficients of aqueous
1004 calcium chloride at 298.15 K, *Journal of Physical and Chemical Reference*
1005 *Data* 6 (1977) 385–408.
- 1006 [86] I. M. Sechenov, Über die konstitution der salzlösungen auf grund ihres
1007 verhaltens zu kohlendioxid solubility of carbon dioxide in water at low
1008 pressure, *Zeitschrift für Physikalische Chemie* 4 (1889) 117–125.
- 1009 [87] S. K. Saxena, *Advances in Physical Geochemistry*, vol. 2, Springer New
1010 York, 1982.
- 1011 [88] A. Schumpe, The estimation of gas solubilities in salt solutions, *Chemical*
1012 *Engineering Science* 48 (1993) 153–158.
- 1013 [89] S. Weisenberger, A. Schumpe, Estimation of gas solubilities in salt solutions
1014 at temperatures from 273 K to 363 K, *AIChE Journal* 42 (1996) 298–300.
- 1015 [90] W. B. Campbell, O. Maass, Equilibria in sulfur dioxide solutions, *Canadian*
1016 *Journal of Research, Section B* 2 (1930) 42–64.
- 1017 [91] T. K. Sherwood, Solubilities of sulfur dioxide and ammonia in water, *Ind-*
1018 *ustrial & Engineering Chemistry* 17 (1925) 745–747.
- 1019 [92] B. Rumpf, G. Maurer, Solubilities of hydrogen cyanide and sulfur dioxide
1020 in water at temperatures from 293.15 to 413.15 K and pressures up to 2.5
1021 MPa, *Fluid Phase Equilibria* 81 (1992) 241–260.
- 1022 [93] S. G. Sayegh, J. Najman, CO₂ - SO₂ brine phase behavior studies, Report
1023 (1984).
- 1024 [94] H.-L. Zhang, G.-H. Chen, S.-J. Han, Viscosity and density of
1025 H₂O+NaCl+CaCl₂ and H₂O+KCl+CaCl₂ at 298.15 K, *Journal of Chem-*
1026 *ical & Engineering Data* 42 (1997) 526–530.

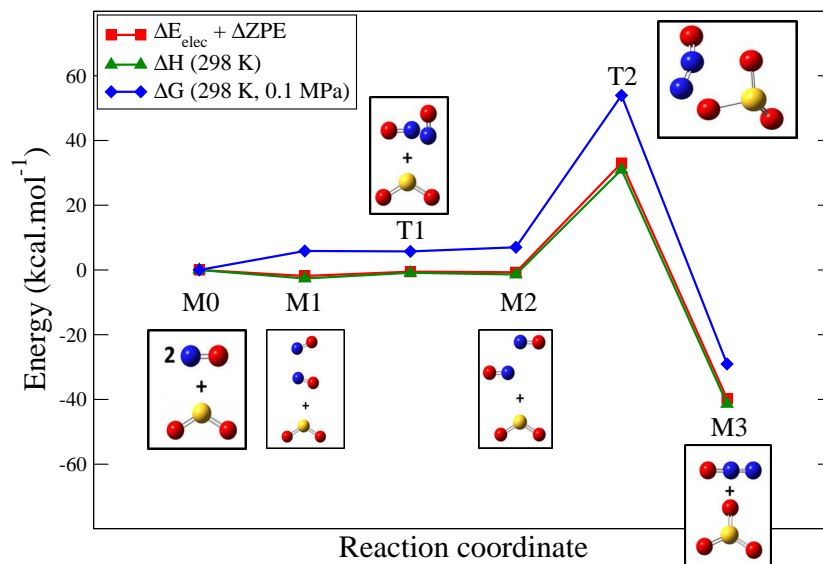


Figure 1: Energy profiles for the $\text{SO}_2 + 2\text{NO} \rightleftharpoons \text{SO}_3 + \text{N}_2\text{O}$ reaction for the electronic energy corrected for the zero point energy (red), the enthalpy at $T = 298 \text{ K}$ (green) and the Gibbs energy at $T = 298 \text{ K}$ and $P = 0.1 \text{ MPa}$ (blue).

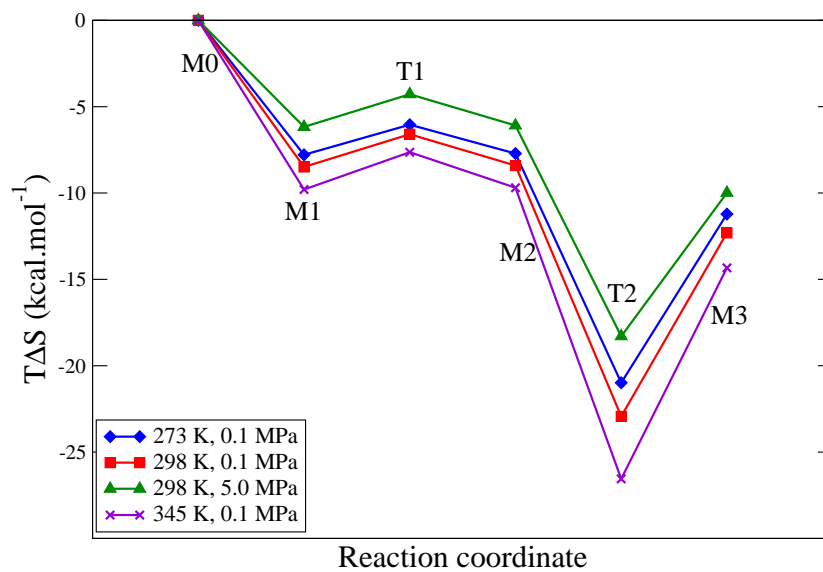


Figure 2: Changes (in kcal.mol⁻¹) of $T\Delta S$ as a function of the reaction coordinate with respect to M0, for 3 temperatures and 2 pressures.

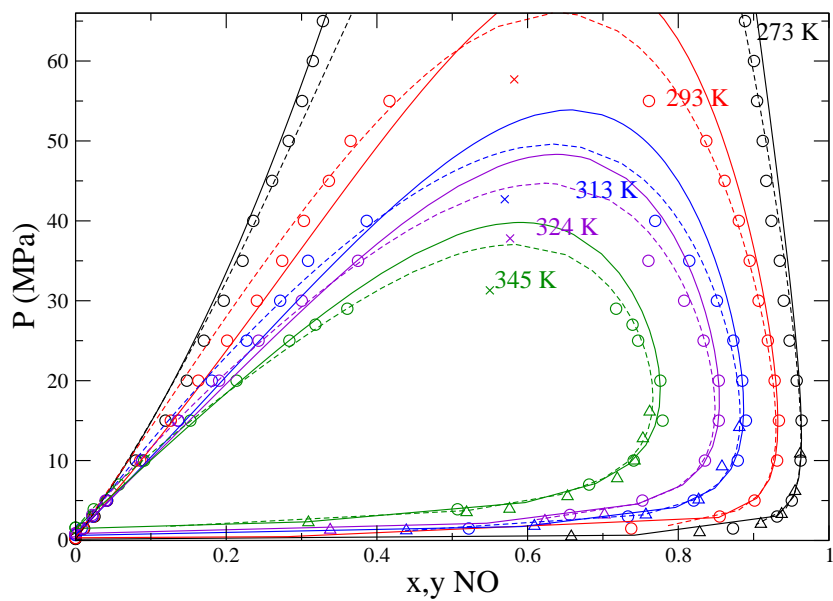


Figure 3: (P, x, y) phase diagrams for the $\text{NO} + \text{SO}_2$ at five temperatures: 273 K (black), 293 K (red), 313 K (blue), 324 K (purple), and 345 K (green). Triangles stand for experimental data (this work and data cited in [16]). Circles denote data obtained using MC molecular simulations, and crosses represent critical points estimated using equations (9) and (10). Lines represent predictions obtained using the PR EoS together with the van Laar model (solid line) and the PR EoS together with the residual part of the Wilson model (dashed line).

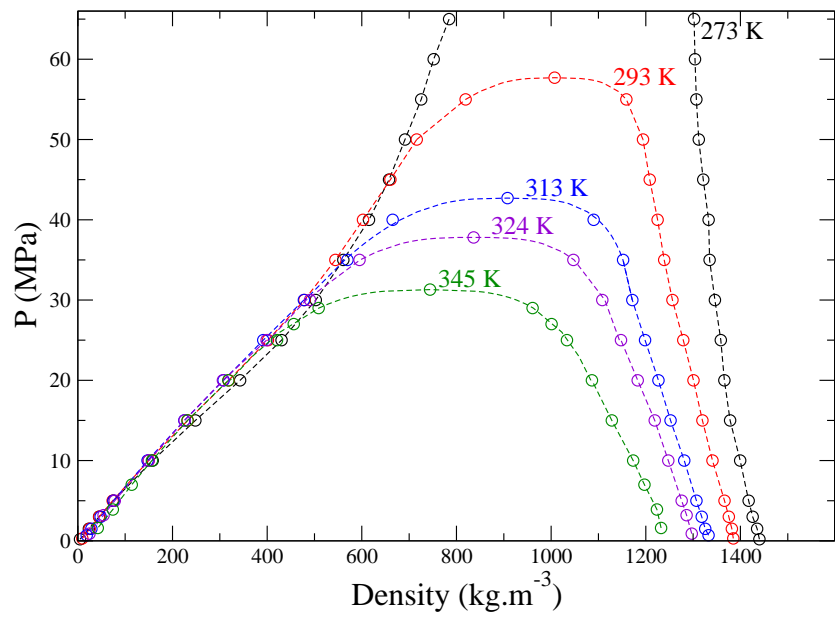


Figure 4: Pressure-density diagrams drawn using data obtained by MC molecular simulations, for the NO + SO₂ at five temperatures: 273 K, 293 K, 313 K, 324 K, and 345 K.

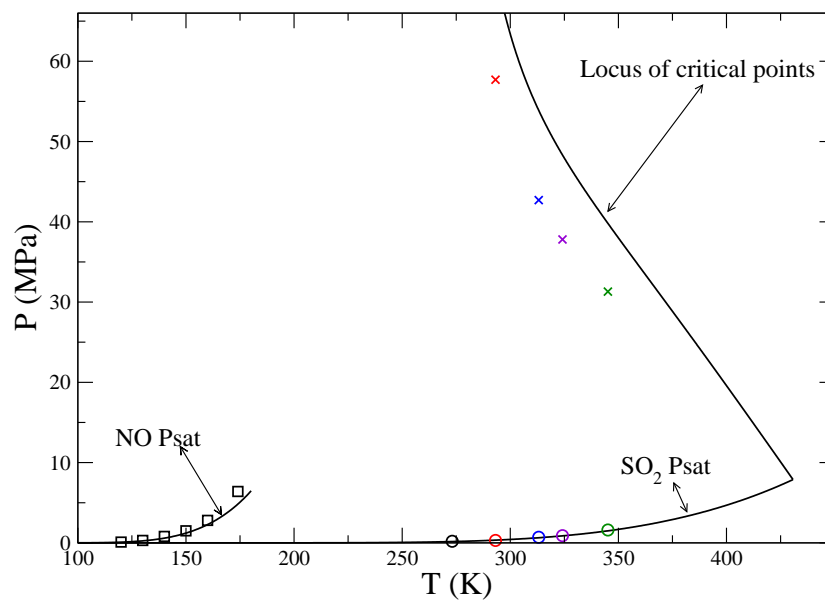


Figure 5: Global pressure-temperature diagram for the NO + SO₂. Lines represent predictions using the PR EoS with the van Laar model, and symbols stand for data obtained using MC molecular simulations at five temperatures: 273 K (black), 293 K (red), 313 K (blue), 324 K (purple), and 345 K (green). NO data for vapour pressure (squares) obtained by MC simulations are taken from our previous work [21].

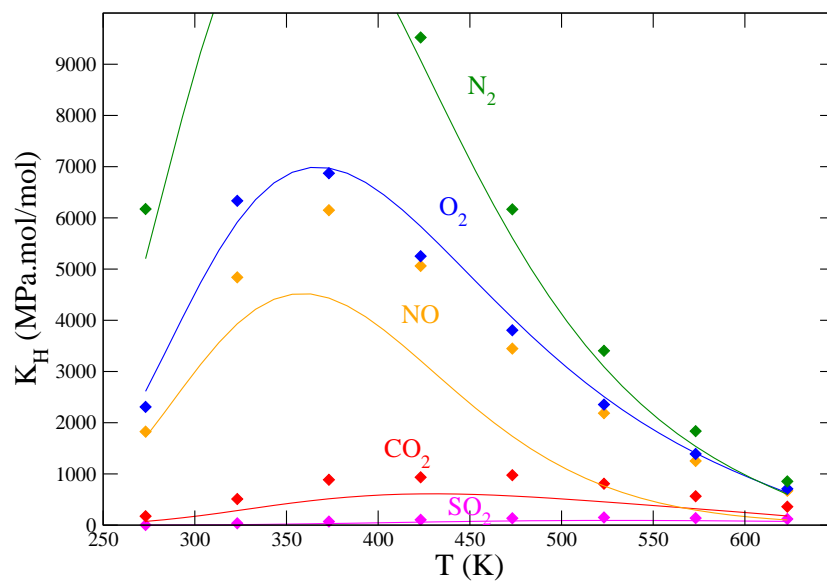


Figure 6: Comparison of simulated Henry constants (diamonds) for SO₂, CO₂, NO, O₂, and N₂ in water, and corresponding curve fitting of experimental values (lines).

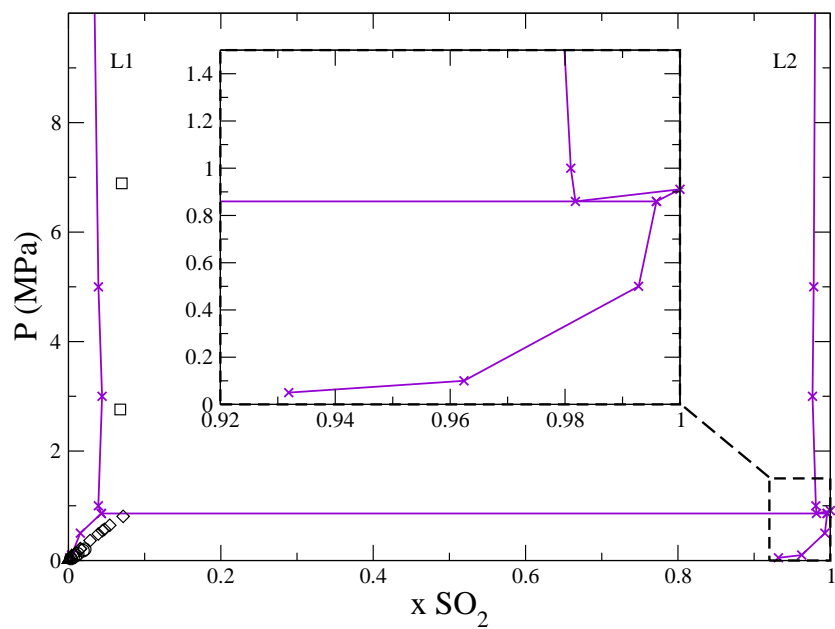


Figure 7: Phase diagrams for $\text{SO}_2 + \text{H}_2\text{O}$ binary mixtures obtained using MC molecular simulations at 323 K (crosses) for pressures up to 10 MPa, and a zoom is proposed on the SO_2 -rich region for pressures up to 1.5 MPa. Experimental data for the H_2O -rich region were extracted from works of Campbell (circles) [90], Sherwood (triangles up) [91], Rumpf (diamonds) [92] and Sayegh (squares) [93], measured at 323 K, 323 K, 333 K, and 318 K, respectively.

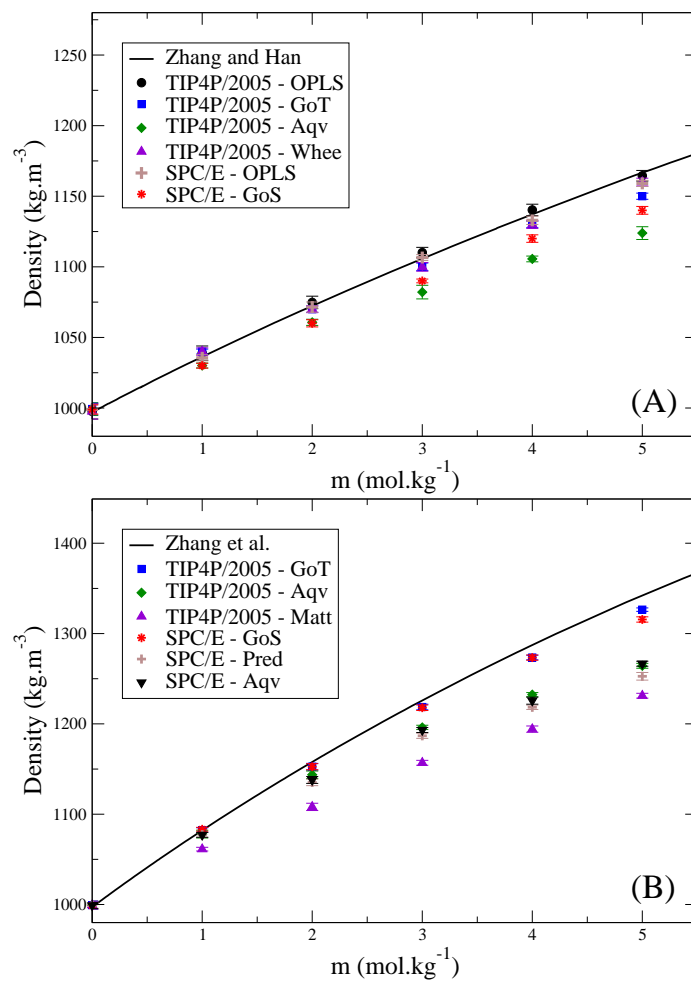


Figure 8: Predicted density values for (A) NaCl (see Table 12) and (B) CaCl₂ (see Table 13) aqueous solutions as a function of the salt molal concentration, at 298 K and 0.1 MPa. The line represents experimental values extracted (A) from the work by Zhang and Han [83] and (B) from the work by Zhang *et al.* [94].

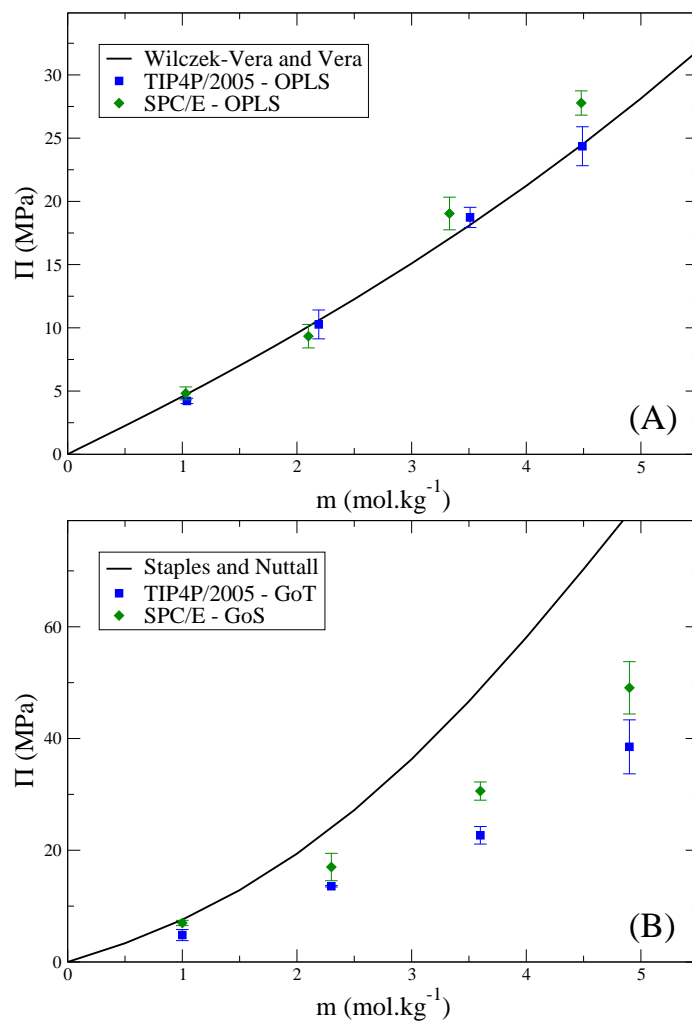


Figure 9: Comparison of experimental and predicted osmotic pressure values for (A) NaCl and (B) CaCl₂ aqueous solutions as a function of the salt molal concentration, at 298 K (see values in Table 14). The line represents experimental values extracted (A) from the work by Wilczek-Vera and Vera [84] and (B) data converted from the work by Staples and Nuttall [85].

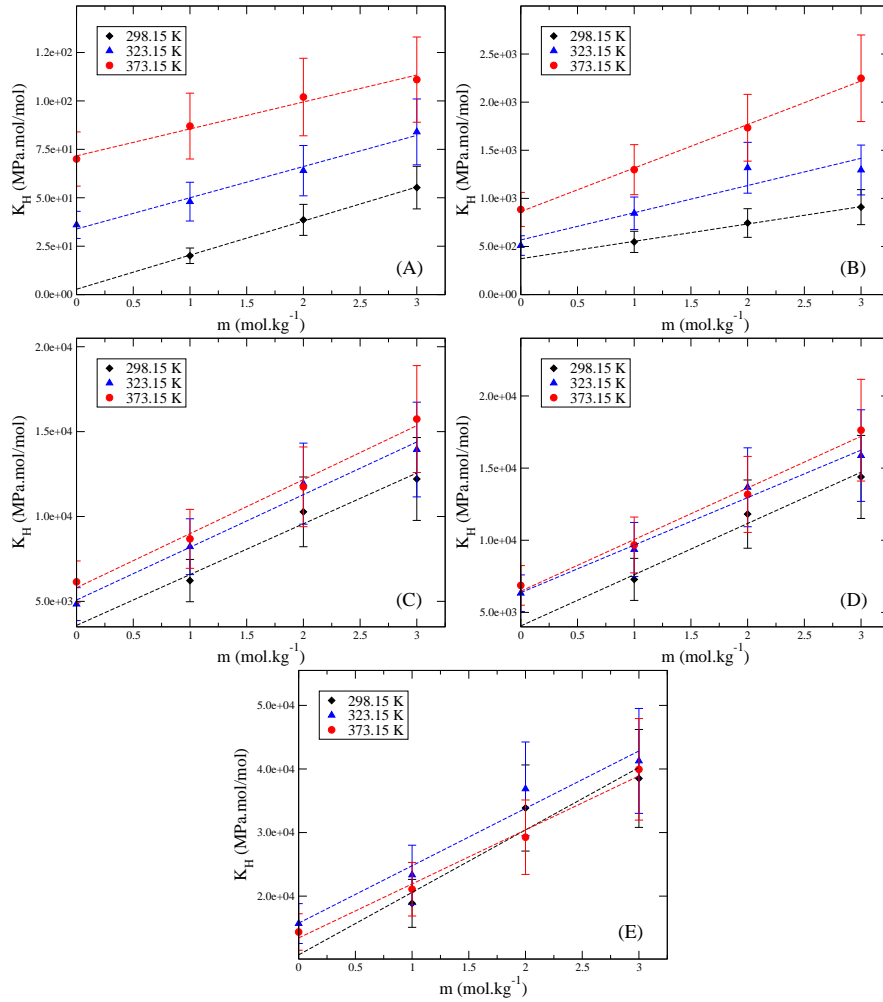


Figure 10: Simulated Henry constant values for SO₂ (A), CO₂ (B), NO (C), O₂ (D), and N₂ (E) in NaCl aqueous solutions as a function of the salt concentration, at 298.15 K (diamonds), 323.15 K (triangles) and 373.15 K (circles).